Analysis of geomagnetic field intensity variations in Mesopotamia during the third millennium BC with archeological implications

Yves Gallet, Michel Fortin, Alexandre Fournier, Maxime Le Goff, Philip Livermore

Analysis of geomagnetic field intensity variations in Mesopotamia during the third millennium BC with archeological implications

Yves Gallet[1], Michel Fortin[2], Alexandre Fournier[1], Maxime Le Goff[1], Philip Livermore[3]

[1] Université de Paris, Institut de Physique du Globe de Paris, CNRS, Paris, France

[2] Faculté des lettres et des sciences humaines, Département des sciences historiques, Université Laval, Québec, Canada

[3] School of Earth & Environment, University of Leeds, Leeds, UK

Abstract

We present new archeointensity results obtained at two multi-layer archeological sites, Tell Atij and Tell Gudeda (northeastern Syria), dated from the Early Bronze Period in the third millennium BC. The archeointensity data were obtained using the experimental protocol developed for the Triaxe magnetometer. In total, 68 fragments (204 specimens) of 151 fragments analyzed passed our selection criteria, allowing average intensity values to be estimated for 14 archeological layers, nine at Tell Atij and five at Tell Gudeda. Based on the available archeological constraints, the different archeological layers of Tell Atij and Tell Gudeda were dated between ~2900 BC and ~2600 BC and between ~2550 BC and ~2325 BC, respectively. The Tell Atij data show a significant increase in intensity over the dated period, while the results from Tell Gudeda exhibit a V-shape evolution. Using high-quality data available from Syria, the Levant and Turkey, a regional geomagnetic field intensity variation curve spanning the entire third millennium BC was constructed using a trans-dimensional Bayesian method. It clearly shows two intensity peaks, around 2600 BC and at ~2300 BC, associated with variation rates of ~0.1-0.2

μT/year. This indicates that the occurrence of century-scale intensity peaks with rates of variation comparable to the maximum rates observed in the modern geomagnetic field is an ubiquitous feature of the geomagnetic secular variation. From an archeological point of view, the new archeointensity data strengthen the hypothesis that the successive occupation of Tell Atij and Tell Gudeda was synchronous with the two first urban phases of Mari, making possible a sustained trade network between these settlements during the third millennium BC. We further suggest that the end of Mari's first urban phase, contemporaneous with the abandonment of Tell Atij, might have been caused by a regional drought episode around 2600 BC. More generally, the Bayesian approach used to estimate the new reference intensity variation curve offers promising chronological constraints for archeological purposes.

Keywords: Archeomagnetism, Archeointensity, Near East, Third millennium BC, Variation rates, Archeological implications

1. Introduction

Archeomagnetism is a unique tool for tracing the detailed evolution of the Earth's magnetic field over the past millennia and, at the same time, for constraining core flow dynamics on time scales ranging from a few tens of years to several millennia. In addition, many examples have shown that once established for a given region, an accurate curve of directional and/or intensity variations of the geomagnetic field provides a powerful chronological tool for archeological purposes. The Near East is undoubtedly an ideal region for the implementation of this dual application of archeomagnetic investigations because it benefits from both extensive archeological

49 and historical data and a growing body of archeomagnetic data, even though the
50 latter are still mainly limited to geomagnetic field intensity variations.

51 In this context, the near-eastern third millennium BC has emerged as a
52 particularly interesting target. From a geomagnetic perspective, Gallet et al (2006;
53 2014) and Gallet and Butterlin (2015) showed the probable existence of two field
54 intensity peaks around 2600 BC and ~2300-2200 BC (see also Ertepinar et al.,
55 2012). These intensity peaks might be linked to archeomagnetic jerks with their
56 possible connection to global field eccentricity and climatic variations (Gallet et al.,
57 2009; Genevey et al., 2013 and references therein), or to geomagnetic spikes
58 described by extreme decadal intensity variation rates (e.g. Shaar et al., 2011; 2016).
59 The extreme variations required by geomagnetic spikes are attracting considerable
60 interest because the intensity variation rates of the order of several μT/year required
61 do not appear compatible with the current understanding of flow dynamics in the
62 outer core, raising therefore many questions about the processes that might produce
63 them (e.g. Livermore et al., 2014). Archeologically speaking, the interest in having a
64 new dating tool for the near-eastern third millennium BC is no less important because
65 this period witnessed in Upper Mesopotamia a succession of major socio-political
66 changes, including the definitive adoption and generalization of urbanism around
67 2600-2500 BC (e.g. Akkermans and Schwartz, 2003) and a major 'crisis of
68 civilization' during the last centuries of this millennium, often seen as a consequence
69 of an episode of severe aridity in the Near East (e.g. Weiss et al., 1993).

70 Knowledge of the predominant geomagnetic field intensity variations in the
71 Near East during the third millennium BC is currently mainly derived from
72 archeointensity data obtained in Mari (modern Tell Hariri), a major Mesopotamian
73 settlement located in the middle Euphrates valley, and in Ebla (modern Tell Mardikh),

another important ancient city further west of modern Syria (Fig. 1; e.g. Gallet et al., 2014, Gallet and Butterlin, 2015). The present study aims to improve the temporal resolution of this record in order to establish a more accurate reference curve and quantify more precisely the intensity variation rates associated with the two intensity peaks previously mentioned. For this purpose, we analyzed ceramic fragments retrieved from two Early Bronze small agricultural settlements, Tell Atij and Tell Gudeda, situated in the middle valley of the Khabur River, a tributary of Euphrates, about 20 km south of the modern town of Hassake in northeastern Syria (Fig. 1). Being granary sites geographically situated between urban centers located further north of the Khabur, like Tell Brak, Tell Mozan and Tell Leilan, and Mari located in the south along the Euphrates River, these two sites also raised interesting questions about their regional role (for a synthesis, see for instance Akkermans and Schwartz, 2003). In this respect, the comparison between the new archeointensity data and those previously obtained in Mari is particularly useful.

2. Archeological contexts and sampling

Tell Atij and Tell Gudeda (λ=36.43°N, φ=40.86°E) are part of a cluster of a dozen of third millennium BC sites, which were excavated in the 1980s by various foreign teams of archeologists owing to the construction of a dam in the middle Khabur Valley (e.g. Fortin, 1991; 2000). These two small tells (mounds) were the subject of five excavation campaigns, from 1986 to 1993, by a Canadian team from Laval University (Québec) headed by Michel Fortin (Fig. 2). Located about 1 km from each other, on both sides of the modern Khabur riverbed, they are multi-layered sites. Tell Atij, ~150 x 40 m, yielded thirteen superimposed occupation layers evidenced in a total thickness of about 9 m, while the 7-m total accumulation at Tell

Gudeda, ~110 x 65 m, produced ten layers. The archeological data excavated from Tell Atij and Tell Gudeda are reported in many publications (e.g. Fortin, 1990a; 1990b; 1994; 1995) and only a very brief overview of these results is provided below.

Based on the presence of plastered room floors and walls, large vaulted and plastered granaries built of mudbricks and grid-planned buildings but with no clear evidence for dwelling units, Tell Atij has been interpreted by Fortin (e.g. 1997; 2001) as a trading outpost where agriculture surplus was concentrated and stored before being redistributed, probably by waterway. A ~3-m thick wall probably reaching a height of ~9 m has surrounded the site since its beginning reflecting its strategic and economical importance. All archeological layers, with thicknesses ranging from ~0.3 m to ~1.0 m, have revealed a dense network of mudbrick walls except in levels VII and VIII that showed no architectural remains and an accumulation of ash layers, which may indicate a marked regression phase of the settlement, or simply the fact that the excavations occurred in an area which was formally a large courtyard that served as a dumping zone. Archeological remains in the top of the mound were poorly preserved because of the emplacement of modern graves. It is worth mentioning that another mound of smaller size (referred to as the 'secondary tell') is present ~100 m to the east of the main tell (from where all potsherds analyzed here were collected). There, the excavations also revealed a series of poorly preserved architectural remains, with perhaps some evidence of a modest port facility, and several tombs. Study of the ceramic material found in Tell Atij and a global analysis of the archeological data from several sites in the Jezirah region allowed dating of the foundation of Tell Atij to be from the beginning of the so-called period Early Jezirah (EJZ) 1 at ~2900 BC and its abandonment likely during the EJZ 2 Final phase, around 2600 BC, thanks to the discovery of both metallic ware and Ninevite 5

excised ceramic fragments in the uppermost (youngest) layer I (Boileau, 2005; Lebeau and Pruss, 2011; Quenet, 2011; Rova, 2011).

Because of the finding of numerous food-baking ovens (for bread?) and basalt grinding tools, Tell Gudeda has been interpreted more as a food-processing site, with again only a few or no firm traces of houses (Fig. 2c,d; Fortin, 1990a; 1990b; 1994; 1995). The thickness of the archeological levels ranged from ~0.3 m to ~1.5 m, with no evidence of a significant break in the occupation. The study of the ceramic material found in Tell Gudeda, showing in particular the total absence of Ninevite 5 excised or incised ceramic fragments in the different archeological layers (Boileau, 2005), while fragments of metallic ware were quite common, indicated that the occupation of this site likely started at the beginning of the EJZ 3a phase, at ~2550 BC, and its abandonment should be placed at the end of the EJZ 3b phase around 2350 BC or slightly after (e.g. Boileau, 2005; Lebeau and Pruss, 2011).

The archeological data showed that the storage and food production capacities in Tell Atij and Tell Gudeda probably exceeded the needs of their own population (remember that no clear dwelling units have been discovered in these two sites) similar to several contemporaneous agricultural settlements excavated in the vicinity (Fig. 1), for instance Tell Raqa'i (Schwartz, 2015) and Tell Ziyadeh (Hole and Tonoike 2016). The discovery of administrative artifacts, such as cylinder seals, and of tokens used to quantify goods has supported the idea that these villages operated under the authority of a centralized political power. The absence of urban centers located nearby in the middle Khabur Valley, however, gave rise to much debate on its identity. The existence of these granary sites has been therefore associated with urban centers located either north, in the upper Khabur valley such as Tell Brak (~50 km away) or south, with Mari on the Euphrates River lying farther, about 200 km

149 downstream (Fig. 1) (e.g. Margueron, 1991; Fortin, 2001). Their main role would then
150 have been the supply in agricultural goods of the populations of these urban centers.
151 Such a north or south connection with distant urban centers was questioned by Hole
152 (e.g. 1991), who instead proposed that the small rural sites of the middle Khabur
153 valley were primarily intended for and ruled by local populations and/or pastoral
154 nomads moving in the area. Akkermans and Schwartz (2003) further emphasized
155 that these villages could be part of a broader regional economic network made of
156 small rural communities interacting with each other without a central authority.

157 At the completion of the archeological campaigns carried out at Tell Atij and
158 Tell Gudeda, a very large collection of pottery fragments (more than ten thousand
159 shards), mostly age-diagnostic ones, has been moved to Laval University where they
160 are properly stored in a research laboratory (http://www.laboarcheologie.ulaval.ca).
161 This is where our archeomagnetic sampling was conducted in February 2018, in
162 which we grouped potsherds found in the same archeological level recovered on
163 both sites. Nine layers were sampled at Tell Atij (layers XIII, XI, IX, VIII, VII, VI, IV, III,
164 I from the oldest to the most recent) and five at Tell Gudeda (layers X, VII, VI, IV, II
165 again with same time ordering). The number of fragments, 151 in total, was
166 distributed among the levels according to the fragments available and to the
167 archeological context, ranging about 10 (in most cases) to about thirty (for layer X of
168 Tell Gudeda). Within any given layer, the shards were assumed to be of the same
169 age (but see below). An important note is that the sampling was only focused on
170 common wares likely produced locally and used for a short time period.

171

172 **3. New archeointensity results**

173 *3.1 Methods*

The archeointensity results were obtained using the experimental protocol developed for the vibrating sample magnetometer called Triaxe (Le Goff and Gallet, 2004). This protocol, which is based on magnetization measurements carried out at high temperatures, aims to reproduce the conditions that led to the acquisition of the natural remanent magnetization (NRM) of the studied samples by acquiring in a single thermal step a new thermoremanent magnetization (the laboratory-TRM), whose direction is exactly parallel to that of the NRM and which replaces most of the original NRM. For a specimen, an intensity value is obtained from the comparison between the magnetization moments of the NRM and the laboratory-TRM measured every ~5°C between two reference temperatures (T1 or T1'>T1 if a secondary magnetization is observed above T1 and T2) where the NRM is strictly uni-directional and represents the magnetization acquired during the manufacture of the ceramic (Le Goff and Gallet, 2004). In particular, the Triaxe protocol allows a sensitive analysis of the magnetization from a large number of measurements over a large temperature interval, which is essential in the case of the combination of several magnetization components, and to take into account the effects of anisotropy and cooling rate on the NRM acquisition (Le Goff and Gallet, 2004 and other references above).

The archeointensity data were selected on the basis of the same selection criteria as those used in all our previous studies (see their summary in Table S1). These criteria aim to test the suitability of the magnetic behavior of the fragments for intensity determination, as well as the consistency of the intensity values obtained at the specimen level. Note that these are independent of another criterion based on the reversibility of the magnetic susceptibility versus temperature curves. These criteria apply both at the fragment level (we analyzed a minimum of 3 specimens per

199 fragment) and at the level of a group of fragments collected from the same
200 archeological layer (with a minimum of three suitable fragments analyzed per
201 archeological level). We recall that the reliability of the archeointensity data derived
202 from the Triaxe protocol has been demonstrated on several occasions from their
203 direct comparison with results obtained using more classical experimental techniques
204 involving magnetization measurements carried out at room temperature (see for
205 example Gallet and Le Goff, 2006; Hartmann et al., 2011; Hervé et al., 2017 and
206 references therein).

207 The studied groups of potsherds were assembled from layers well defined
208 both from stratigraphic and archeological viewpoints. Within a given archeological
209 layer, the ages of the different shards are distributed within the age range considered
210 for the layer, without it being possible to know the shape of the distribution. In
211 addition, the possibility that some fragments incidentally moved in the stratigraphy
212 cannot be excluded, i.e. their age would not correspond to that of the archeological
213 layer where they were found (see for instance a discussion in Yutsis-Akimova et al.,
214 2018). The displacement of potsherds from one layer to another may have been
215 caused by several phenomena, such as the digging into a lower layer by new settlers
216 to set up their new installations, the tunneling by burrowing animals after
217 abandonment of the site or simply erosion factors that had a great effect in particular
218 on Tell Atij, considering that more than half of the site has been washed away by the
219 river flowing near-by. Similar severe erosion phenomenon occurred at Tell Gudeda.
220 To take this difficulty into account, and following Yutsis-Akimova et al (2018), we
221 applied a 3σ rejection test to the intensity values obtained from the fragments from all
222 groups (i.e. all layers). Here we considered that up to 25% of the fragments from the
223 same group could possibly be outliers on the basis of the 3σ test, which roughly

corresponds to the same rejection rate as in Yutsis-Akimova et al. (2018). The corresponding intensity values could therefore be eliminated from the calculation of the mean intensity characteristic of the layer.

3.2 Description of the new data

The Triaxe analyses yielded archeointensity values meeting the selection criteria for 36 of the 81 fragments from Tell Atij and 32 of the 70 fragments from Tell Gudeda. The corresponding success rates of ~44% and ~46%, respectively are relatively low compared to our previous studies (e.g. Gallet et al., 2014; Gallet and Butterlin, 2015). This is largely due to the frequent presence of several magnetization components likely related to the use of the studied ceramics for cooking purposes, leading to secondary heating at a temperature generally lower than that of the initial firing achieved during the manufacture of the pottery. As a result, intensity determinations were often obtained at high temperatures (T1' >~300°C; Table S2). Examples of thermal demagnetization data are shown in Fig. S1.

The magnetization of the Tell Atij and Tell Gudeda fragments is likely mainly carried by a mineral of the titanomagnetite family, with often a small fraction of a high coercivity magnetic phase, probably hematite. This dual composition is demonstrated by isothermal remanent magnetization (IRM) acquisition curves up to 1.5 T (Fig. S2) and by the thermal demagnetization of three-axis IRM acquired in fields of 0.2 T, 0.4 T and 1.5 T (Fig. 3). The magnetic mineralogy deduced from the IRM experiments is very homogeneous for the entire collection of fragments. In addition, magnetic susceptibility versus temperature curves acquired for all fragments, although more variable in shape, further confirm the good stability of the magnetization on heating

248 (already deduced from the Triaxe measurements) within the same temperature range
249 as that used for intensity analyses (up to ~500°C; Fig. 4).

250 All intensity values obtained at the fragment level are based on the averaging
251 of the R'(Ti) data (see definition in Le Goff and Gallet, 2004) acquired from three
252 different specimens. In summary: the R'(Ti) data for each specimen represent all
253 ratios between the NRM and laboratory-TRM fractions demagnetized between T1 (or
254 T1') and the running temperature Ti increasing from T1 (or T1') and T2 with a
255 temperature step of ~5°C, multiplied by the field intensity applied for laboratory-TRM
256 acquisition. Examples of archeointensity data obtained for six groups of fragments
257 are reported in Fig. 5 (each individual curve in the different diagrams shows the
258 intensity R'(Ti) data and the temperature intervals at which they were obtained, used
259 to estimate a mean intensity value at the specimen level). Several diagrams in Fig. 5
260 show the presence of outlying data, as defined by the use of the 3σ rejection test
261 (Fig. 5a,d,f; Fig. 6). Outliers were detected for seven layers, three at Tell Atij (Fig. 6a)
262 and four at Tell Gudeda (Fig. 6b). In six of the seven layers, a single outlier was
263 observed. A difference concerns layer X of Tell Gudeda where three outliers were
264 detected. Situated at the base of the Tell, placed on virgin soil, and cleared over a
265 small area on the edge of the Tell (and on the erosion limit), we were aware that
266 some fragments could have come from erosion of the upper layers. This problem
267 was anticipated by sampling many more fragments for this layer (note that 15
268 intensity values were obtained for this level while the number of data varied from
269 three to seven for all other layers; see Table 1). This represents a rejection rate of
270 20% while the rates vary from 15% to 25% in the other six layers. It should be noted
271 that these deviating values are nevertheless in agreement with the evolution of the
272 intensity values observed through the two archeological sequences (i.e. they are

consistent with the range of values found in the two sequences), which argue for a displacement of the concerned shards in the stratigraphy (and thus in time) of their site (Fig. 6). As previously indicated, all the deviating values were eliminated from the calculation of the intensity means at the group level (red squares, Fig. 6). Thanks to this consistency test, the mean intensity values hence obtained are particularly well defined, with between 3 and 12 independent fragments. The intensity values range between ~40 μT and ~56 μT, with standard deviations ranging from 0.2 μT to 4.5 μT (with a mean of ~2 μT), or between ~1% and ~9% of the corresponding mean values (average of ~4%) (Table 1 and Table S2).

4. Age modeling and field intensity variations

For the sake of simplicity, age models for the Tell Atij and Tell Gudeda data have been determined using a bootstrap approach relying on 10000 random draws. The chosen parameters were the following: i) indetermination of ± 10 cm on the exact position of the boundaries between the different archeological layers, and therefore of ± 20 cm in the thickness of these layers; and ii) dating of the upper and lower bounds of the sequences arbitrarily established with a standard deviation of 25 years, thus leading to age uncertainties on these tie-points of ± 50 years at 95% confidence level. Considering the archeological constraints, the upper/lower bounds were respectively chosen at 2900 ± 25 BC and 2600 ± 25 BC for Tell Atji, and at 2550 ± 25 BC and 2325 ± 25 BC for Tell Gudeda. Furthermore, instead of simply using the approximation of a constant accumulation rate all through the archeological sequences, we considered reasonable random variations in the accumulation rate up to 20% of the average accumulation rate provided at a given random draw by the ratio between the total thickness of the sequence and the total time included in the

298 sequence (Fig. S3). Note that this model essentially makes it possible to estimate
299 reasonable age uncertainties for the new data, i.e. comparable to those of most other
300 results available in the Near East.

301 The data obtained at Tell Atij show an increase in geomagnetic field intensity
302 of about 15 μT, between ~40 μT around 2850 BC and ~55 μT around 2500 BC (Fig.
303 7). This increase appears to be continuous, however, it can be noted that the
304 intensity values obtained for layers VI to XI are very similar, which could indicate that
305 these levels correspond to short and close time intervals. The contrast with the
306 archeointensity values obtained for the three most recent layers (I, III and IV), which
307 show a marked increase, suggests either a longer temporal spacing between these
308 levels (a possibility that cannot be tested given the way the age model was
309 established) or higher intensity variation rates during the corresponding period. The
310 latter option could be supported by the fact that the standard deviations associated
311 with the mean intensity values are larger for those layers. The archeointensity data
312 obtained at Tell Gudeda also show a marked evolution of the intensities (Fig. 7),
313 characterized by a V shape, with variations of the order of 10 μT between the highest
314 values (~55 μT; layers X and II), at the beginning (~2600 BC) and towards the end
315 (~2350 BC) of the site occupation, and the lowest values (~45 μT) around 2450 BC
316 (layers IV, VI and VII).

317

318 **5. Construction of a near-eastern geomagnetic field intensity variation curve**
319 **for the third millennium BC**

320 In addition to the data from Ebla and Mari, a few other archeointensity results
321 meeting standard (and 'modern') quality criteria, which attest the stability of the

322 magnetic mineralogy of the studied fragments during thermal treatment and take into
323 account the anisotropy and cooling rate effects on TRM acquisition, were obtained in
324 Syria for the third millennium BC, from Mashnaqa (Gallet and Le Goff, 2006) and Tell
325 Mozan (Stillinger et al., 2015). In our study, we decided to select only high-quality
326 data available in a geographical area as close as possible to Northeastern Syria, in
327 order to construct a reference mean intensity variation curve focused on the Near-
328 East (or the Upper Mesopotamian region). This led us to consider the results
329 obtained in Tel Hazor and Tel Megiddo (Israel; Shaar et al., 2016), Arslantepe
330 (Southeastern Turkey; Ertepinar et al., 2012) and in Kültepe (Central Turkey;
331 Ertepinar et al., 2016), at ~550 km, ~470 km and ~670 km from Mari, respectively. To
332 make the archeointensity data obtained from pottery fragments statistically more
333 equivalent, we averaged them by (homogeneous) archeological context, yielding
334 group-mean intensity values as those reported in this study (Table 1). Of particular
335 note are the data obtained in Tel Hazor and Tel Megiddo, where a total of four mean
336 intensity values with ages ranging from ~3000 BC to ~2150 BC could each be
337 estimated from a minimum of three fragments collected from independent pottery.
338 This approach, however, led to the rejection of the data obtained at Tell Mozan on
339 isolated fragments. In total, we selected 48 data covering the third millennium BC
340 (Fig. 7; Table S3).

341 To construct a reference geomagnetic field intensity variation curve for the Near
342 East encompassing the entire third millennium BC, we used the method recently
343 developed by Livermore et al. (2018), which imposes a minimum regularization on
344 the reference curve. Here the degree of temporal complexity of the models is fixed by
345 the data themselves, through the use of a trans-dimensional Bayesian technique
346 relying on piecewise linear interpolation of the data between internal vertices guided

by both experimental and age uncertainties and possibly by a time-order relationship between some of them (as is the case for the new datasets from Tell Atij and Tell Gudeda). The method delivers a time-dependent posterior distribution of the intensity data, as computed from a large set of individual models, characterized by mean, median and modal models and a 95% credible interval (see description and discussion in Livermore et al., 2018; https://www.github.com/plivermore/AH-RJMCMC). To create the posterior distribution, a Reverse-Jump Monte Carlo Markov Chain procedure was implemented, in which the data ages are incorporated as "age hyper-parameters" into the model vector (leading to the procedure referred to as AH-RJMCMC). Note that this approach is particularly well suited for the recovery of rapid intensity variations, as seems to be the case in the Near East during the third millennium BC.

An example posterior intensity variation curve is shown in Fig. 7 by its average and 95% credible interval (note that the archeointensity data were all transferred to Mari's latitude using the virtual axial dipole moment approximation). This figure reveals a relatively tight 95%-confidence envelope, indicating that the available results taken as a whole form a fairly consistent dataset. It allows us to clearly isolate two geomagnetic field intensity peaks, with maxima dated around 2550 BC and ~2300 BC and a minimum dated at ~2400 BC, further confirming the fact that the occurrence of century-scale intensity peaks is an ubiquitous characteristic of the secular variation.

6. Discussion

6.1 On the robustness of the geomagnetic field intensity variation curve and rates of change

The distribution of the available data, taking into account their age and intensity uncertainties, with respect to the 95%-confidence envelope of the intensity evolution computed by the AH-RJMCMC method shown in Fig. 7, indicates that several results may be considered as outlying. This mainly concerns two data obtained in Tel Hazor (Israel) with large age uncertainties (ΔT=300 years) and mean ages at ~2650 BC and ~2150 BC (violet circles, Fig. 7; Shaar et al., 2016) and the result from Kültepe (2400 ± 50 BC; yellow triangle, Fig. 7; Ertepinar et al., 2016). With respect to the Tel Hazor data, their most likely dating derived from their marginal age distributions lies in the old and recent parts of their corresponding prior age intervals, respectively (Fig. S4a,b). On the other hand, the most likely dating of the Kültepe result obtained from burnt adobe bricks (their magnetization is therefore posterior to the construction of the building concerned) is strongly confined to the younger part of its prior age interval (Fig. S4c).

In a second calculation, we chose to eliminate the three highlighted data above (Fig. 8a; Table S4). The resulting mean curve is very similar to that of Fig. 7. It is also almost identical to the curve constructed using only the results from Mari, Ebla, Mashnaqa, Tell Atij and Tell Gudeda, the latter forming a very homogeneous data collection (Triaxe protocol and same averaging approach) (Fig. S5). The similarity between the different curves indicates that the estimates are robust and do not strongly depend on a few data. It is also important to specify that the estimated mean curve is very insensitive to the chosen Markov chain sampling parameters, such as the maximum number of vertices allowed, the length of the calculation chain, or the maximum and minimum intensity values used to bound the calculation, which further underlines its robustness.

The intensity values calculated at Mari from the global geomagnetic field model

397 referred to as SCHA.DIF.14k (Pavón-Carrasco et al., 2014) show similar fluctuations
398 but with smaller amplitude compared to those retrieved by considering only the
399 regional archeointensity data (Fig. 8a). However, the uncertainties associated with
400 the results obtained using the SCHA-DIF.14k model are such that a constant
401 geomagnetic intensity (of about 45 μT) over the entire third millennium BC lies within
402 the error bounds. Such a behavior is inconsistent with the new curves reported in Fig.
403 7, 8a because of their more pronounced temporal variations and tighter error bounds.
404 This discrepancy, which is typical for such comparisons (e.g. Genevey et al., 2016),
405 illustrates the still limited resolution of the global archeomagnetic field reconstructions
406 compared to detailed regional curves. This difference occurs despite the fact that the
407 SCHA.DIF.14k model, constructed using only archeological and volcanic data,
408 probably has, among all available models, one of the best accuracies for the northern
409 hemisphere where most of the available data are located.

410 From the posterior model ensemble shown in Fig. 8a, we then estimated the
411 corresponding evolution of the variation rates (Fig. 8b). Note that for each model of
412 the ensemble, the intensity curve is interpolated on a regular grid with a constant
413 spacing equal to ~5 years, regardless of the number and location of the internal
414 vertices of this specific model. The slope of each interpolated intensity curve is
415 computed locally at each point of the regular (in time) grid. This provides us with the
416 variation rates (dF/dt) for any given member of the ensemble. Finally, given the
417 ensemble of dF/dt curves, it is straightforward to estimate the mean, median curves
418 and the credible interval of dF/dt. The variation rates associated with the two intensity
419 peaks from the third millennium BC attain, on average, values of ~0.10-0.20 μT/year.
420 While these values are significantly lower than those proposed for geomagnetic
421 spikes, they are very similar to (or even slightly higher than) the maximum variation

422 rates observed in the recent field (e.g. Livermore et al., 2014). They also appear
423 similar to other variation rates previously determined from archeomagnetic data of
424 different ages obtained in Mesopotamia (6th millennium BC; Yutsis-Akimova et al.,
425 2018) and in Western Europe (past three millennia; e.g. Genevey et al., 2016; Hervé
426 et al., 2017). With the exception of the geomagnetic spikes, values of the order of 0.1
427 to 0.3 μT/yr might therefore represent typical and recurrent intensity variation rates,
428 which would not require a specific and unusual geodynamo behavior.

429

430 *6.2 Comparison with previous data from Mari and archeological implications*

431 The archeological data suggest that the occupation of Tell Atji and Tell
432 Gudeda was synchronous with the first and second urban phases of Mari,
433 respectively (e.g. Margueron, 2004), with the trend of the new archeointensity data
434 being broadly in agreement with existing understanding of the time-dependent
435 intensity (Fig. 7). A good consistency is indeed observed between the Tell Atij
436 dataset and the results previously obtained for Mari's first urban phase (Genevey et
437 al., 2003; Gallet et Le Goff, 2006; Gallet et Butterlin, 2015). The main difference
438 concerns the most recent intensity values, that obtained at Mari being lower than the
439 one obtained at Tell Atij. The probable reason for this discrepancy has already been
440 discussed by Gallet and Butterlin (2015): the last occupation level(s) of Mari's first
441 urban phase remain undocumented as they were leveled during the construction of
442 Mari's second urban phase (e.g. Margueron, 2004) implying a gap in the record
443 around 2600 BC.

444 Concerning Tell Gudeda, the intensity value characterizing its earliest
445 occupation is in very good agreement with the two intensity data obtained for the
446 beginning of Mari's second urban phase (Fig. 7). A decreasing trend is next observed

447 in both sequences, although the Tell Gudeda dataset exhibits a more pronounced
448 minimum in intensity around 2450 BC. The new dataset likely allows the resolution of
449 the previous record to be increased. In contrast, the archeointensity value obtained
450 toward the end of the occupation of Tell Gudeda (layer II) is significantly higher than
451 the two data documenting the end of Mari's second urban phase. This may be
452 explained by the fact that the latter data predate the very end of this phase, coming
453 from a level of occupation stratigraphically below that marking the destruction of the
454 city with a violent burning (Margueron, 2004; Butterlin, 2010). For the same reason,
455 they are also lower than the intensity results obtained at Ebla in the context of the
456 destruction of Palace G (Gallet et al., 2014), while the destruction of Ebla and Mari by
457 the Akkadian troops was likely very close in time.
458 The new archeointensity data therefore strengthen the fact that the successive
459 occupation of Tell Atij and Tell Gudeda was synchronous with the two first urban
460 phases of Mari. This makes possible a sustained economic relationship between
461 these settlements during the third millennium BC. An inscribed tablet discovered in
462 Mari proved the existence of economic interactions between Mari during its third and
463 last urban phase (~2200-1750 BC) and the Middle Khabur region, intended for the
464 supply of Mari in cereals (Margueron, 1991). The persistence of these interactions
465 throughout Mari's history could easily be explained by the fact that Mari was located
466 in a semi-arid to arid area where, despite the practice of irrigation agriculture,
467 meeting the needs of the population was a permanent challenge. Furthermore, the
468 very existence of Mari can be understood only by the determination to control the
469 economic exchanges, in particular for wood and ores, between the northern regions
470 (Anatolia, the Taurus Mountains and the Upper Mesopotamia) and Southern
471 Mesopotamia transiting through the Euphrates. The power of Mari would have been

472 stronger when the city was assured of a regular supply in agricultural products
473 necessary for its livelihood, especially in drought years.

474 Sustained economic interactions between these sites throughout the third
475 millennium BC is in little doubt, but their form is much more uncertain, ranging
476 between a relationship of pure domination assuring the exclusivity of the agriculture
477 surplus in favor of Mari and a more flexible association established on the basis of
478 regular trade agreements with local people (for discussion, see for instance Fortin,
479 1988; 2000; Margueron, 1991; 2004; Hole, 1991; Akkermans and Schwartz, 2003).
480 Additionally, it is tempting to link the abandonment of Tell Atij to that of Mari (end of
481 its first urban phase) around 2600 BC. In this case, enhanced drought stress and
482 induced environmental changes in Upper Mesopotamia, in the so-called 'zone of
483 uncertainty' (Wilkinson et al., 2014), around the middle of the third millennium BC
484 might appear as a plausible causal factor (e.g. Gallet et al., 2006; see a more general
485 discussion in Kaniewski et al., 2012). Several geochemical and petrographic datasets
486 could argue in favor of such a climate (aridity)-related feature (e.g. Riehl et al., 2014;
487 Cheng et al., 2015; see also discussion in Issar and Zohar 2004 and references
488 therein), further coinciding in time with a brief drifting ice maximum in the North
489 Atlantic belonging to Bond event #3 (Bond et al., 2001).

490

491 *6.3 Application of the AH-RJMCMC method to archeological dating*

492 Thanks to its accuracy and strong fluctuations, the new reference geomagnetic
493 field intensity variation curve offers a promising tool for archeomagnetic dating and
494 temporal calibration between the different and independent archeological
495 chronologies that have been established so far in the Near East.

To further illustrate this issue, we applied the AH-RJMCMC algorithm to derive the marginal age distributions of the Tell Atij and Tell Gudeda results, using the same dataset as in Fig. 8a. A uniform age distribution between the upper and lower age limits of each sequence slightly extended to take into account the 1σ uncertainties considered to construct the age model discussed in Section 4 were used as priors for the data obtained at Tell Atij and Tell Gudeda. Here the crucial element is the strict time-order relationship between the different archeological layers in each sequence (see discussion in Livermore et al., 2018). As two examples, the joint posterior probability distributions of the age and intensity value for Groups AT02 from Tell Atij and GD02 from Tell Gudeda are reported in Fig. 9a (left and right panel, respectively). Starting from the initial large age interval between 2925 and 2575 BC and between 2575 and 2300 BC considered as a prior, the marginal posterior distribution for the data ages favors respectively an age interval between 2925 and 2747 BC (mean age 2839 BC) for Group AT02 and between 2349 and 2300 BC (mean age 2317 BC) for GD02. On the other hand, in the two cases, the posterior intensity is almost identical to the prior.

The posterior age determinations reported by two methods, respectively with the age model discussed in Section 4 (filled symbols) and without the age model but assuming broad bounds as above (white symbols) are shown in Fig. 9b. The differences between the two series of results, which illustrate the information provided by the age model, are relatively minor, being of less than ~30 years for all groups of fragments (22 years on average). Both in Tell Atij and Tell Gudeda, the mean posterior mean ages calculated without the age model are systematically younger compared to the mean posterior ages calculated with the age model by a roughly constant age shift. This means that the posterior ages calculated without age

modeling argue in favor of a fairly constant accumulation rate through both sequences as is independently assumed in Fig. 7,8.

Another remark can be made concerning group GD02 from Tell Gudeda. Its posterior age distribution, which is strongly confined to the youngest part of its prior age interval, could indicate that the site was still occupied after 2300 BC (Fig. 9a), during the beginning of the Akkadian period. Such a feature would be in accordance with the discovery of extremely rare Akkadian-type potsherds in the late-most layer of the site (Boileau, 2005). These are examples of information that could be submitted for archeologists' consideration, while recognizing that this information may evolve with future improvements in the archeointensity database.

7. Conclusions

The third millennium BC in the Near East is a particularly favorable period to illustrate the applications of archeomagnetism to both geomagnetism and archeology.

As regards to geomagnetism, we show that this period was marked by two geomagnetic field intensity peaks, whose maxima were reached around 2600 BC and 2300-2200 BC, characterized by rates of change of ~0.10-0.20 μT/year. These are rapid variations with respect to the recent geomagnetic field but seem to be recurrent in the Near East, as well as in Europe, over the past millennia.

From an archeological point of view, the new archeointensity data obtained at Tell Atij and Tell Gudeda, two rural settlements located in the Middle Khabur Valley, are in agreement with the archeological data that attest to the fact that the occupation of these two sites has been contemporary respectively with the first and second urban phase of Mari located about 200 km further south along the Euphrates River.

On the basis of the available archeological, historical and environmental data, and now archeomagnetic data, it therefore seems possible that these archeological sites were part of the same trade network during the third millennium BC in Upper Mesopotamia. We also suggest that the temporary abandonment of Mari, synchronous with the permanent abandonment of Tell Atij around 2600 BC was caused by a brief regional episode of aridity.

Finally, this study also allows us to illustrate the potential of the Bayesian AH-RJMCMC method recently developed by Livermore et al. (2018), which by computing probability distributions for the data ages together with the intensity variation with time, provides new dating constraints for archeological artifacts based on their archeointensity signature.

Acknowledgements

We are grateful to Jean Margueron, Pascal Butterlin, Sophie Cluzan and Agnès Genevey for very helpful discussions. Thanks to Yohan Guyodo for his help in acquiring IRM and hysteresis data. We also thank two anonymous reviewers for their helpful comments on the manuscript. This study was financed by INSU-CNRS program PNP and by the Simone and Cino Del Duca Foundation of the French Academy of Science. This is IPGP contribution no. *xxxx*.

References

Akkermans, P.M.M.G., Schwartz, G.M., 2003. The Archaeology of Syria. From Complex Hunter-gatherers to Early Urban Societies (ca. 16,000–300 BC). Cambridge World Archaeology, Cambridge University Press, New York, pp. 467.

569 Boileau, M.-C., 2005. Production et distribution des céramiques au IIIième millénaire
570 en Syrie du Nord-Est. Epistèmes Ed., Paris, pp. 94.

571 Bond, G., Kromer, B., Beer, J., Muscheler, R., Evans, M., Showers, W., Hoffmann,
572 S., Lotti-Bond, R., Hajdas, I., Bonani, G., 2001. Persistent solar influence on North
573 Atlantic climate during the Holocene. Science 294, 2130–2136.

574 Butterlin, P., 2010, Cinq campagnes à Mari : nouvelles perspectives sur l'histoire de
575 la métropole du Moyen Euphrate, CRAI 2010, 1, 171-229.

576 Cheng, H., Sinha, A., Verheyden, S., Nader, F.H., Li, X. L., Zhang, P. Z., Yin, J. J.,
577 Yi, L., Peng, Y. B., Rao, Z. G., Ning, Y. F., Edwards, R. L., 2015. The climate
578 variability in northern Levant over the past 20,000 years. Geophys. Res. Lett. 42,
579 8641-8650.

580 Ertepinar, P., Langereis, C.G., Biggin, A.J., Frangipane, M., Matney, T., Ökse, T.,
581 and Engin, A., 2012, Archeomagnetic study of five mounds from Upper Mesopotamia
582 between 2500 and 700 BC: Further evidence for an extremely strong geomagnetic
583 field ca. 3000 years ago, Earth Planet. Sci. Lett. 357-358, 84-98.

584 Ertepinar, P., Langereis, C.G., Biggin, A.J., de Groot, L.V., Kulakoglu, Omura, S.,
585 2016, Full vector archaeomagnetic records from Anatolia between 2400 and 1350
586 BCE: Implications for geomagnetic field models and the dating of fires in antiquity.
587 Earth Planet. Sci. Lett. 434, 171-186.

588 Fortin, M., 1988. Rapport préliminaire sur la première campagne de fouilles
589 (printemps 1986) à tell 'Atij, sur le moyen Khabour (Syrie). Syria 65, 139-171.

590 Fortin, M., 1990a. Rapport préliminaire sur la seconde campagne de fouilles à Tell
591 Atij et la première à tell Gudeda (automne 1987), sur le moyen Khabour. Syria 67,
592 219-256.

593 Fortin, M., 1990b. Rapport préliminaire sur la 3ème campagne de fouilles à tell 'Atij et
594 la 2ème à tell Gudeda, sur le Khabour (automne 1988). Syria 67, 535-577.

595 Fortin, M., 1991. Récentes recherches archéologiques dans la moyenne vallée du
596 Khabour, Syrie. La société canadienne des études mésopotamiennes. Bulletin 21,
597 Lost civilizations of the desert. Recent archeological research in third millennium
598 North Syria, 5-15.

599 Fortin, M., 1994. Rapport préliminaire sur la quatrième campagne à tell 'Atij et la
600 troisième à tell Gudeda (printemps 1992). Syria 71, 361-396.

601 Fortin, M., 1995. Rapport préliminaire sur la cinquième campagne à tell 'Atij et la
602 quatrième à tell Gudeda (printemps 1993). Syria 72, 23-53.

603 Fortin, M., 1997. Urbanisation et “redistribution” de surplus agricoles en
604 Mésopotamie septentrionale (3000-2500 av. J.-C.). In: Aspects of urbanism in
605 antiquity, Aufrecht W. et al. (Eds.) Sheffield Academinc Press, Sheffield, 50-81.

606 Fortin, M., 2000. Economie et société dans la moyenne vallée du Khabour durant la
607 période de Ninive 5. In: La Djéziré et l'Euphrate syriens de la protohistoire à la fin du
608 II^{e} millénaire av. J.-C. Tendances dans l'interprétation historique des données
609 nouvelles, Rouault, O. Wäfler, M. (Eds), Subartu 8, Brepols, Turnhout, 111-136.

610 Fortin, 2001, Mise en valeur des terres de la moyenne vallée du Khabour au 3^{e}
611 millénaire. In: Conquête de la steppe et appropriation des terres sur les marges
612 arides du Croissant fertile, Geyer, B. (Ed.), Travaux de la Maison de l’Orient
613 Méditerranéen vol. 36, Maison de l'Orient Méditerranéen, Lyon, 27-54.

614 Gallet, Y., Le Goff, M., 2006. High-temperature archeointensity measurements from
615 Mesopotamia. Earth Planet. Sci. Lett. 241, 159-173.

616 Gallet., Y., Genevey., A., Le Goff, M., Fluteau, F., Eshraghi, S.A., 2006. Possible
617 impact of the Earth's magnetic field on the history of ancient civilizations. Earth
618 Planet. Sci. Lett. 246, 17-26.

619 Gallet, Y., Le Goff, M., Genevey, A., Margueron, J., and Matthiae, P., 2008,
620 Geomagnetic field intensity behavior in the Middle East between ~3000 BC and
621 ~1500 BC, Geophys. Res. Lett., 35, L02307.

622 Gallet, Y., Hulot, G., Chulliat, A., Genevey, A., 2009. Geomagnetic field hemispheric
623 asymmetry and archeomagnetic jerks. Earth Planet. Sci. Lett. 284, 179-186.

624 Gallet, Y., D'Andrea, M., Genevey, A., Pinnock, F., Le Goff, M., Matthiae, P., 2014.
625 Archaeomagnetism at Ebla (Tell Mardikh, Syria). New data on geomagnetic field
626 intensity variations in the Near East during the Bronze Age. J. Archaeol. Sci. 42, 295-
627 304.

628 Gallet, Y., Butterlin, P., 2015. Archaeological and geomagnetic implications of new
629 archaeomagnetic intensity data from the Early Bronze high terrace "Massif Rouge" at
630 Mari (Tell Hariri, Syria). Archaeometry 57 Suppl. 1. 263-276.

631 Genevey, A., Gallet, Y., Margueron, J.-C., 2003, Eight thousand years of
632 geomagnetic field intensity variations in the eastern Mediterranean, J. Geophys.
633 Res., 108 (B5), 2228.

634 Genevey, A., Gallet, Y., Thébault, E., Jesset, S., Le Goff, M., 2013. Geomagnetic
635 field intensity variations in Western Europe over the past 1100 years. Geochem.
636 Geophys. Geosyst. 14/8, 2858-2872.

637 Genevey, A., Gallet, Y., Jesset, S., Thébault, E., Bouillon, J., Lefèvre, A., Le Goff, M.,
638 2016. New archeointensity data from French Early Medieval pottery production (6th–

639 10th century AD). Tracing 1500 years of geomagnetic field intensity variations in
640 Western Europe. Earth Planet. Sci. Lett. 257, 205-219.

641 Hartmann, G., Genevey, A., Gallet, Y., Trindade, R., Le Goff, M., Najjar, R.,
642 Etchevarne, C., Afonso, M., 2011. New historical archeointensity data from Brazil :
643 Evidence for a large regional non-dipole field contribution over the past few centuries.
644 Earth Planet. Sci. Lett. 306, 66-76.

645 Hervé, G., Fassbinder, J., Gilder, S., Metzner-Nebelsick, C., Gallet, Y., Genevey, A.,
646 Schnepp, E., Geisweid, L., Pütz, A., Reub, S., Wittenborn, F., Flontas, A., Linke, R.,
647 Riedel, G., Walter, F., Westhausen, I., 2017. Fast geomagnetic field intensity
648 variations between 1400 and 400 BCE: new archaeointensity data from Germany.
649 Phys. Earth Planet. Inter. 270, 143-156.

650 Hole, F., 1991. Middle Khabur settlement and agriculture in the Ninevite 5 period. La
651 société canadienne des études mésopotamiennes, Bulletin 21, Lost civilizations of
652 the desert. Recent archeological research in third millennium North Syria, 17-29.

653 Hole, F., Tonoike, Y. (Eds.), 2016. Homesteads of the Khabur: Tell Ziyadeh and
654 other settlements. BAR Inter. Series 2827, Oxford, p. 511.

655 Issar, A. S., Zohar, M., 2004. Climate change -Envrionment and civilizations in the
656 Middle East. Springer, New York, p. 252.

657 Kaniewski, D., Van Campo, E., Weiss, H., 2012. Drought is a recurring challenge in
658 the Middle East, PNAS 109, 3862-3867.

659 Lebeau, M., Pruss, A., 2011. Introduction. Associated Regional Chronologies for the
660 Ancient Near East and the Eastern Mediterranean (ARCANE) vol. 1 Jezirah, Lebeau
661 M. (Ed.), Brepols Pub., 1-17.

662 Le Goff, M., Gallet, Y., 2004. A new three-axis vibrating sample magnetometer for
663 continuous high-temperature magnetization measurements: applications to paleo-
664 and archeo-intensity determinations. Earth Planet. Sci. Lett. 229, 31-43.

665 Livermore, P.W., Fournier, A., Gallet, Y., 2014. Core-flow constraints on extreme
666 archeomagnetic intensity changes. Earth Planet. Sci. Lett. 387, 145-156.

667 Livermore, P.W., Fournier, A., Gallet, Y., Bodin, T., 2018. Transdimensional
668 inference of archeomagnetic intensity change. Geophys. J. Int. 215, 2008-2034.

669 Lowrie, W., 1990. Identification of ferromagnetic minerals in a rock by coercivity and
670 unblocking temperatures properties. Geophys. Res. Lett., 17, 159–162.

671 Margueron, J.-C., 1991. Mari, l'Euphrate, et le Khabour au milieu du IIIe millénaire.
672 La société canadienne des études mésopotamiennes, Bulletin 21, Lost civilizations of
673 the desert. Recent archeological research in third millennium North Syria, 79-100.

674 Margueron, J.-C., 2004, Mari Métropole de l'Euphrate au IIIe et au début du IIe
675 millénaire av. J.-C., A. Picard and J. Picard eds, Association pour la Diff. de la
676 Pensée Fr., Paris, pp. 575.

677 Pavón-Carrasco, F. J., Osete López, M. L., Torta, J. M., De Santis, A., 2014. A
678 geomagnetic field model for the Holocene based on archaeomagnetic and lava flow
679 data. Earth Planet. Sci. Lett., 388, 98–109.

680 Quenet, 2011. Stratigraphy. Associated Regional Chronologies for the Ancient Near
681 East and the Eastern Mediterranean (ARCANE) vol. 1 Jezirah, Lebeau M. (ed.),
682 Brepols Pub., 19-47.

683 Riehl, S., 2012. Variability in ancient Near Eastern environmental and agricultural
684 development. J. Arid Environments. 86, 113-121.

685 Riehl, S., 2014. Drought stress variability in ancient Near Eastern agricultural
686 systems evidenced by $\delta^{13}C$ in barley grain. PNAS 111, 12348-12353.

687 Rova, E., 2011. Ceramic. Associated Regional Chronologies for the Ancient Near
688 East and the Eastern Mediterranean (ARCANE) vol. 1 Jezirah, Lebeau M. (ed.),
689 Brepols Pub., 49-127

690 Schwartz, G. M. (Ed.), 2015. Rural archaeology in early urban Mesopotamia:
691 excavations at Tell Al-Raqa'i. Cotsen Inst. of Archeology UCLA, Monumenta
692 Archaeologica, p. 696.

693 Shaar, R., Ben-Yosef, E., Ron, H., Tauxe, L., Agnon, A., Kessel, R., 2011.
694 Geomagnetic field intensity: how high can it get? How fast can it change? Constraints
695 from iron-age copper-slag. Earth Planet. Sci. Lett. 301, 297-306.

696 Shaar, R., Tauxe, L., Ron, H., Ebert, Y., Zuckerman, S., Finkelstein, I., Agnon A.,
697 2016. Large geomagnetic field anomalies revealed in Bronze to Iron Age
698 archeomagnetic data from Tel Megiddo and Tel Hazor, Israel. Earth Planet. Sci. Lett.
699 442, 173-185.

700 Stillinger, M. D., Feinberg, J. M., Frahm, E., 2015 Refining the Archaeomagnetic
701 Dating Curve for the Near East: New Intensity Data from Bronze Age Ceramics at
702 Tell Mozan, Syria. J. Archaeol. Sci. 53, 345-355

703 Weiss, H, Courty, M.-A., Wetterstrom, W., Guichard, F., Senior, L., Meadow, R.,
704 Curnow, A., 1993. The Genesis and Collapse of Third Millennium North
705 Mesopotamian Civilization. Science 261, 995-1004.

706 Wilkinson, T. J., Philip, G., Bradbury, J., Dunford, R., Donoghue, D., Galiatsatos, N.,
707 Lawrence, D., Ricci, A., Smith, S. L., 2014. Contextualizing early urbanization:

settlement cores, early states and agro-pastoral strategies in the Fertile Crescent during the fourth and third millennia BC. J. World Prehist. 27, 43-109.

Yutsis-Akimova, S., Gallet, Y., Amirov, S., 2018. Rapid geomagnetic field intensity variations in the Near East during the 6th millennium BC: New archeointensity data from Halafian site Yarim Tepe II (Northern Iraq). Earth Planet. Sci. Lett. 482, 201-212.

715

716 **Figure and table captions**

717

718 **Fig. 1.** General map of the Near East and location of several major archeological
719 sites (red circles) and of several modern towns (blue circles). The location of Tell Atij
720 and Tell Gudeda is indicated by the yellow star.

721

722 **Fig. 2.** Photos of Tell Atij (a) and Tell Gudeda (b). © Mission archéologique de Tell
723 Atij.

724

725 **Fig. 3.** Magnetic properties of the studied pottery fragments. Examples of thermal
726 demagnetization of three-axis isothermal remanent magnetization (IRM) acquired in
727 fields of 0.2 T (squares), 0.4 T (circles) and 1.5 T (triangles).

728

729 **Fig. 4.** Examples of low field magnetic susceptibility versus temperature curves
730 acquired up to 510°C. The red (blue) curve shows the evolution during heating
731 (cooling).

732

733 **Fig. 5.** Examples of archeointensity data obtained from three groups of fragments
734 from Tell Atij (a,b,c) and from Tell Gudeda (d,e,f). Each curve in the different panels
735 shows the R'(Ti) data obtained for one specimen over the temperature range
736 considered for intensity determination (see text).

737

738 **Fig. 6.** Mean archeointensity data obtained at the fragment and group levels from
739 Tell Atij (a) and Tell Gudeda (b). The data are reported as a function of their
740 stratigraphic and archeological layers. The blue circles show the data obtained at the
741 fragment level, which were considered for group-mean computation. Data eliminated
742 on the basis of a 3σ test are shown by the white circles. The red squares indicate the
743 mean intensity values derived at the group level.

744

745 **Fig. 7.** Archeointensity results dated from the third millennium BC selected in the
746 Near East (see text and details on the figure). All values were transferred to the
747 latitude of Mari (λ=34.55°N). The mean curve and its 95% credible interval (blue
748 curve and shaded area) were estimated using the AH-RJMCMC method developed
749 by Livermore et al. (2018). The computational parameters are σ_{move} = 30
750 years, σ_{change} = 5 μT, σ_{birth} = 5 μT for the model pertubations, one datum age is
751 perturbed per age-resampling step from the prior, K_{max}=150 (the maximum number of
752 change points), priors of 15 μT for the intensity minimum and 100 μT for the intensity
753 maximum and a chain length of 100 million samples (see explanations in Livermore
754 et al., 2018). The age interval of the three successive urban phases in Mari (Mari
755 I/II/III) is also shown at the top of the figure.

756

757 **Fig. 8.** Near-eastern geomagnetic field intensity variation curve (a) and rates of
758 variations dF/dt (b) determined for the third millennium BC, characterized by their
759 mean and 95% credible interval (blue curve and shaded area), after removing three
760 outlying results from the dataset used in Fig. 7 (see text). The curves were
761 constructed using the AH-RJMCMC method with the same computational parameters

762 as in Fig. 7. For comparison, the intensity values and their uncertainties estimated at
763 Mari, Syria from the global geomagnetic field model SCHA.DIF.14k constructed by
764 Pavón-Carrasco et al. (2014) are also exhibited in panel (a) (orange curve and
765 shaded area).

766 **Fig. 9.** Posterior dating results derived from the AH-RJMCMC algorithm (Livermore
767 et al., 2018). (a) Joint posterior probability distribution of the marginal age and
768 intensity of two groups of fragments, AT02 from Tell Atij (left panel) and GD02 from
769 Tell Gudeda (right panel) (see text). The prior and posterior age distributions of the
770 ages (top) and intensities (right) are displayed in orange and green, respectively. (b)
771 Comparison between the posterior ages calculated with and without the use of an
772 age model for the Tell Atij and Tell Gudeda results (same dataset as in Fig. 8; see
773 text). The posterior marginal age distributions (mean ages and their 95% credible
774 interval) derived without the age model are shown as white unfilled symbols. The
775 shaded areas in red and green indicate the extent of the prior age intervals used for
776 the Tell Atij and Tell Gudeda data, respectively. The filled symbols show the mean
777 posterior mean ages calculated with the age model discussed in Section 4.

778 **Table 1.** Group-mean archeointensity data obtained in Tell Atij and Tell Gudeda
779 before (column 6) and after (column 7) the use of a 3σ-rejection test. The data
780 identification is provided in the first column, and information on their archeological
781 and stratigraphic position is provided in columns 2 and 3. Their dating (column 4)
782 derives from the age model discussed in the text. Column 5 indicates the number of
783 fragments (specimens) used to compute the mean intensity values before applying
784 the 3σ test. The last column shows the intensity values after the 3σ test transferred to
785 the latitude of Mari.

786

Supplementary material

Fig. S1. Examples of thermal demagnetization of the NRM carried by 9 specimens (5 from Tell Atij and 4 from Tell Gudeda) obtained during the Triaxe experiments. Open (close) circles refer to the inclinations (declinations). The red circles indicate the directions obtained at temperature T1'. The R'(T1) (open circles) and R'(T1') (close circles) data obtained for the same specimens are also shown to the right of the demagnetization data.

Fig. S2. Normalized IRM acquisition curves obtained in fields up to 1.5 T. The data from two fragments of each group (archeological layer) are reported in the diagram.

Fig. S3. Age calibration of the different archeological layers in Tell Atij (a) and Tell Gudeda (b) according to the modeling described in the text.

Fig. S4. Joint posterior probability distribution of the marginal age and intensity of three groups of fragments discussed in Section 6.1. (a) Tel Hazor, layer XVIII, (b) Tel Hazor, layer XX, (c) Kültepe, KT12. In each panel, the prior and posterior age distributions of the ages (top) and intensities (right) are displayed in orange and green, respectively. The computations were carried out using the age model described in Section 4 for the Tell Atij and Tell Gudeda data.

809 **Fig. S5.** (a) Intensity variation curve (mean and 95% credible interval) determined for
810 the third millennium BC using only Syrian archeointensity data from Mari, Ebla,
811 Mashnaqa, Tell Atij and Tell Gudeda (same symbols and same computational
812 parameters as in Fig. 7). (b) Corresponding evolution of the intensity variation rates
813 (mean and 95% credible interval).

814

815 **Table S1.** Selection criteria applied to the Triaxe archeointensity determinations (see
816 further discussion in Le Goff et al., 2004 et Genevey et al., 2016).

817

818 **Table S2.** Archeointensity data obtained in Tell Atij and Tell Gudeda at the specimen,
819 fragment and group levels. T1-T2, Temperature interval (in °C) for intensity
820 determination; Hlab, laboratory field used for TRM acquisition; NRM T1' (%), fraction
821 of NRM involved from T1' in intensity determination (with T1<T1'<T2); Slope R' (%),
822 slope of the R'(Ti) data within the temperature interval of analysis; F, intensity value
823 in μT derived per specimen; F mean value per fragment ± σ, mean intensity in μT
824 computed per fragment with its standard deviation. Group F mean value ± σ, mean
825 intensity in μT computed for each group of fragments. Group F mean value after 3σ
826 test ± σ, mean intensity in μT computed for each group of fragments after the use of
827 a 3σ-rejection test. Note that the fragments eliminated on the basis of this test are
828 indicated by a * in the second column.

829

830 **Table S3.** Selection of 48 intensity data spanning the third millennium BC used to
831 compute the posterior intensity variation curve shown in Fig. 7. Following recent
832 archeological consideration, note that the dating of one result from Mashnaqa and

five data from Mari were slightly revised with respect to their original publication (indicated by a * in the third column).

Table S4. Posterior intensity variation curves (averages and 95% credible intervals) of intensities and rates of changes shown in Fig. 8 as derived from the trans-dimensional Bayesian procedure developed by Livermore et al. (2018). Details of the computational parameters are provided in legend of Fig. 7.

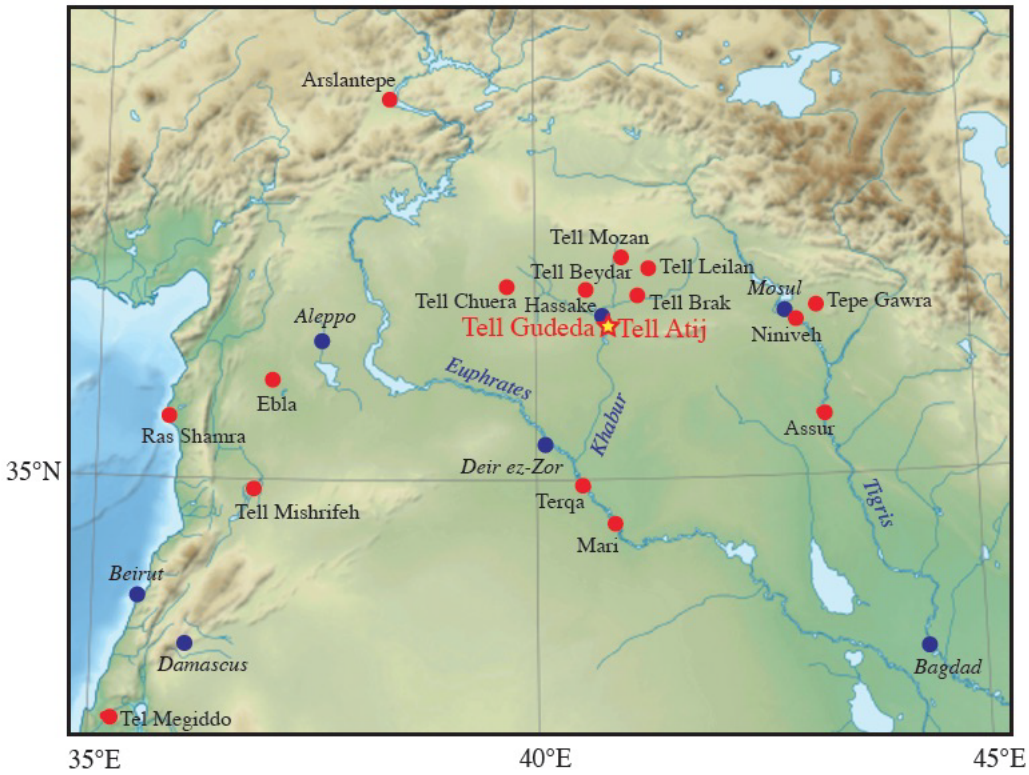
Arslantepe
Tell Mozan
Tell Beydar
Tell Leilan
Tell Chuera
Hassake
Tell Brak
Mosul
Tepe Gawra
Niniveh
Aleppo
Tell Gudeda
Tell Atij
Euphrates
Khabur
Ebla
Ras Shamra
Assur
Deir ez-Zor
Tigris
Terqa
Tell Mishrifeh
Mari
Beirut
Damascus
Baghdad
Tel Megiddo
35°N
35°E
40°E
45°E

Figure 1

Figure 2

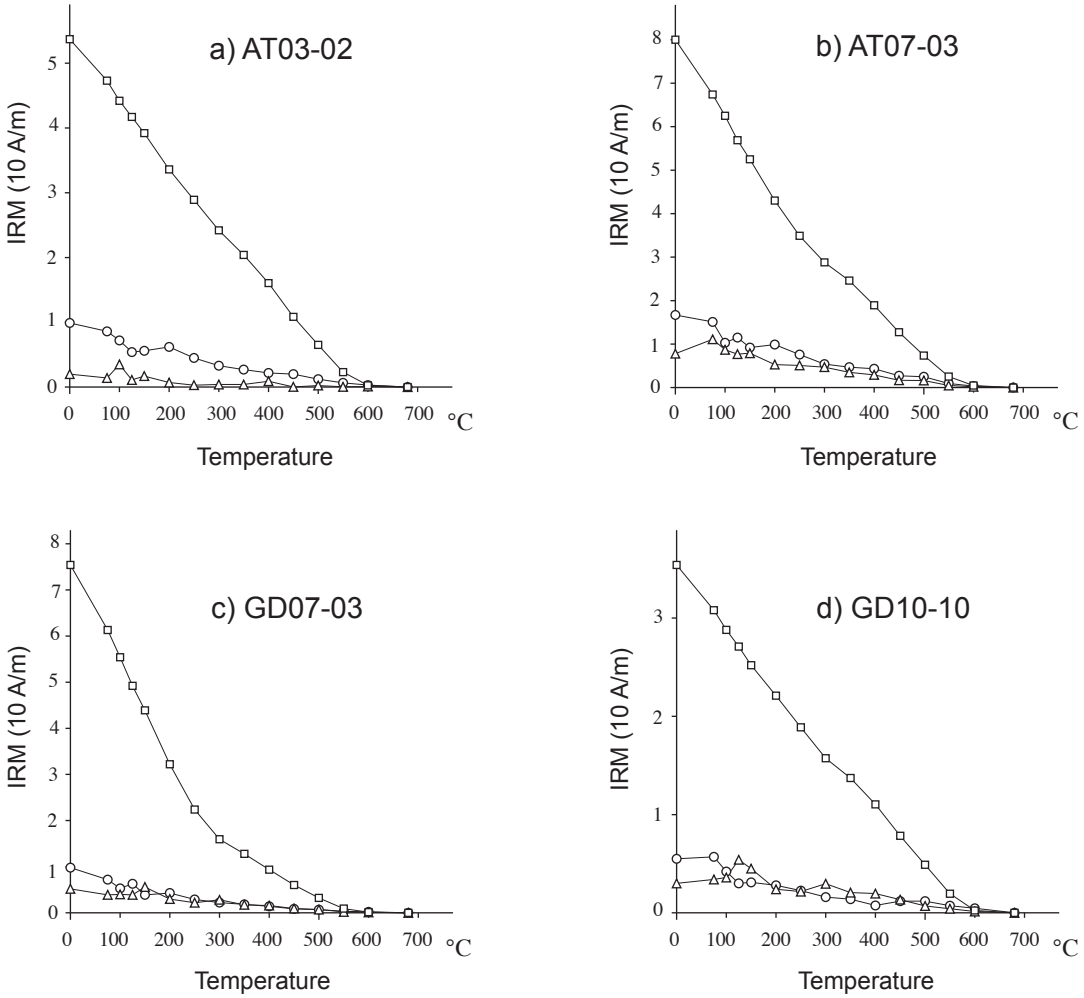
a) AT03-02
b) AT07-03
c) GD07-03
d) GD10-10
IRM (10 A/m)
Temperature
°C
0
100
200
300
400
500
600
700

Figure 3

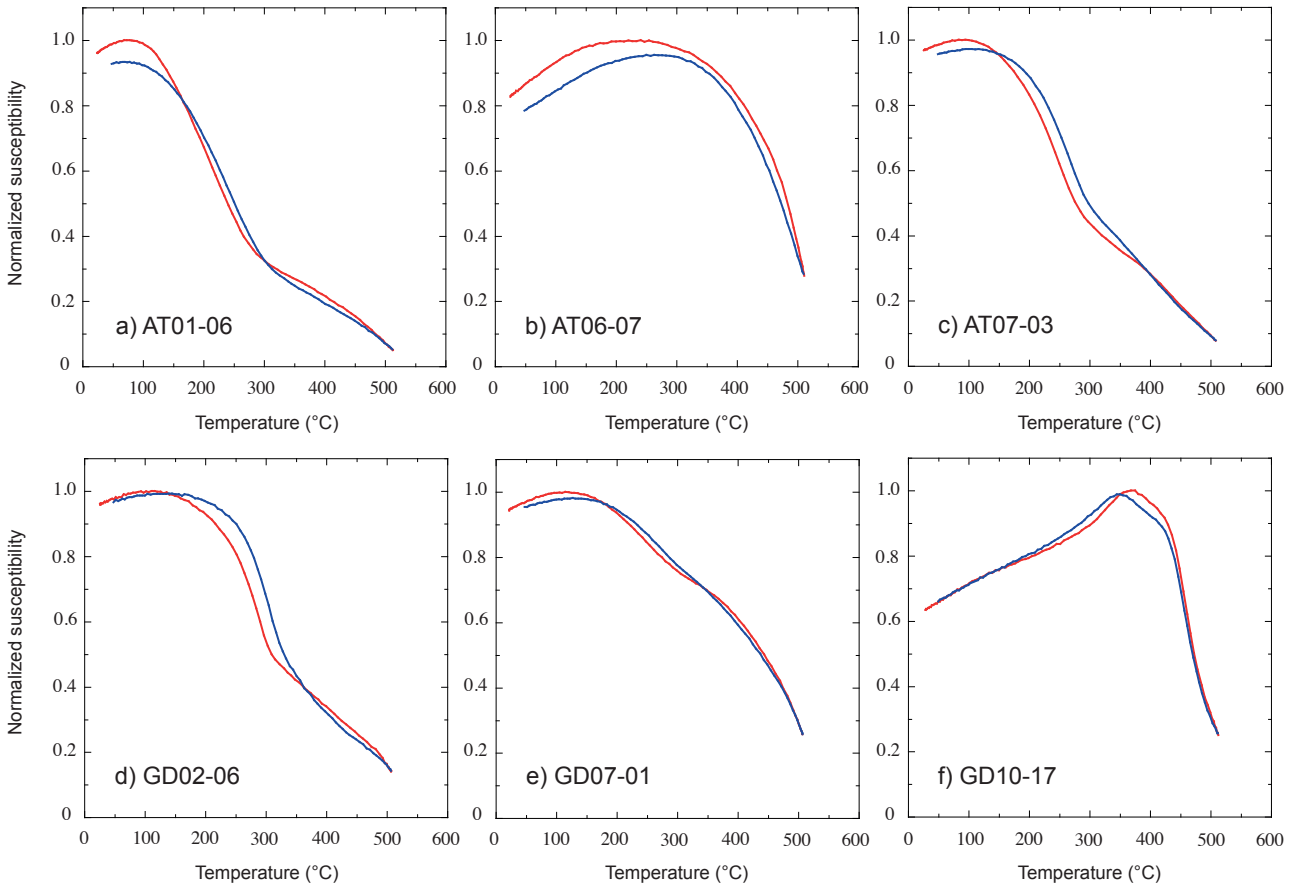
Normalized susceptibility
a) AT01-06
b) AT06-07
c) AT07-03
d) GD02-06
e) GD07-01
f) GD10-17
Temperature (°C)
0
0.2
0.4
0.6
0.8
1.0
0
100
200
300
400
500
600

Figure 4

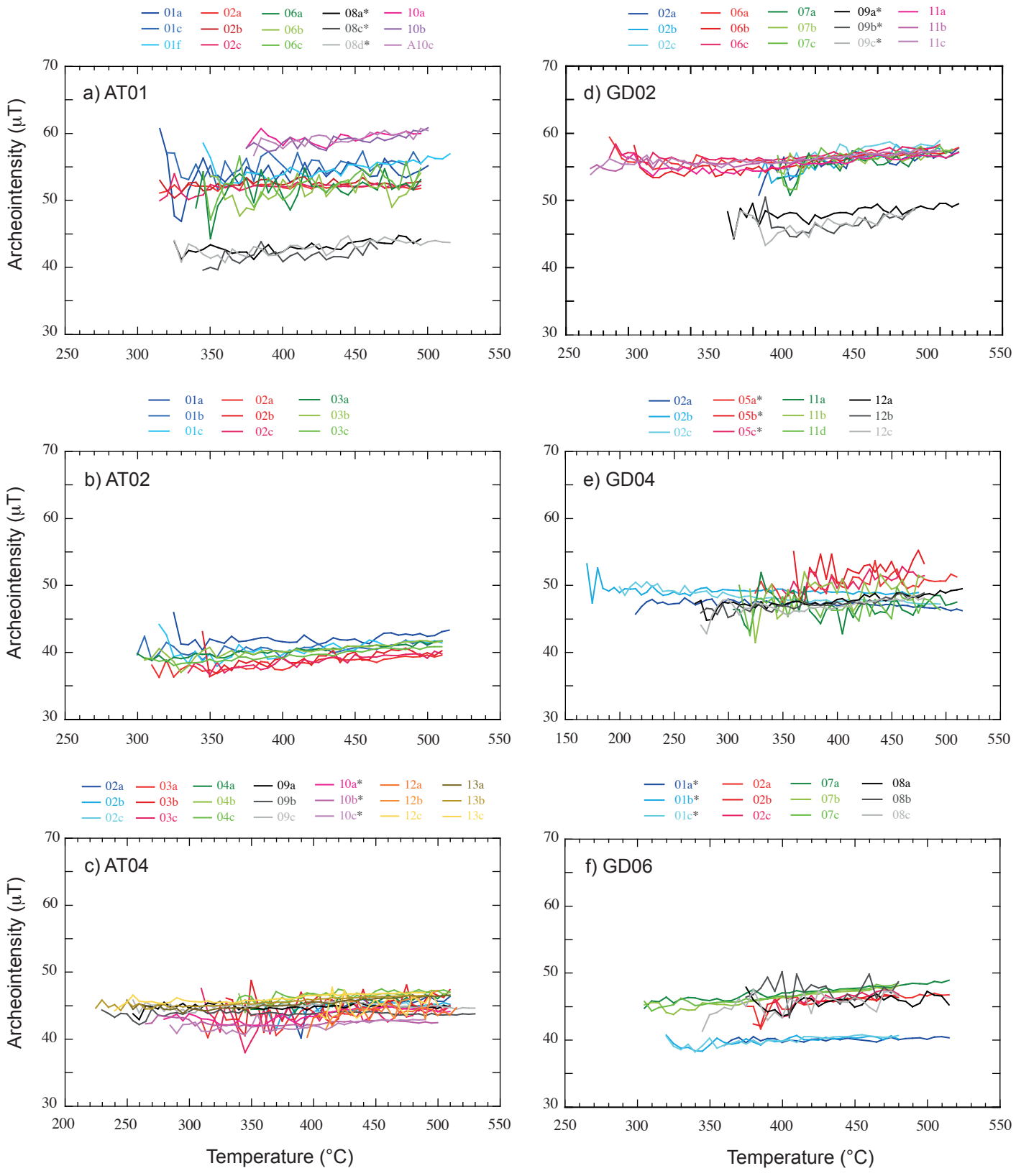
a) AT01
b) AT02
c) AT04
d) GD02
e) GD04
f) GD06
Archeointensity (μT)
Temperature (°C)

Figure 5

a) Tell Atij

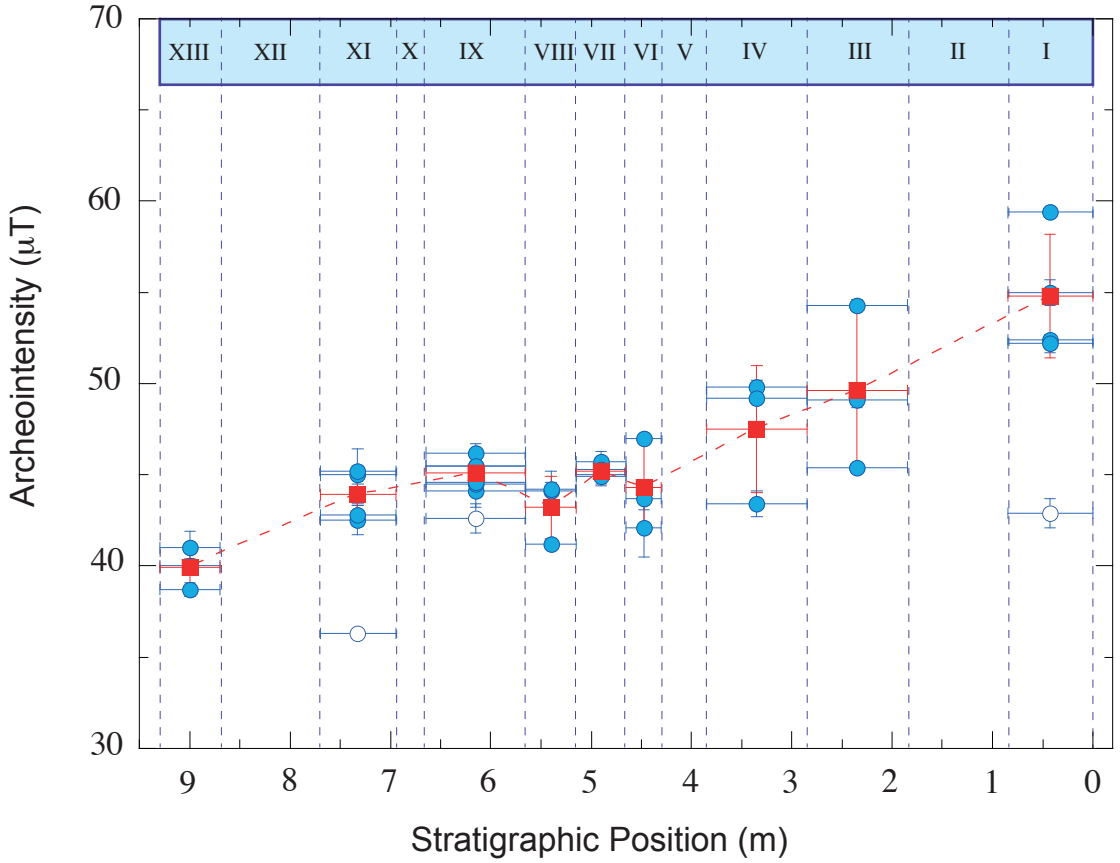

b) Tell Gudeda

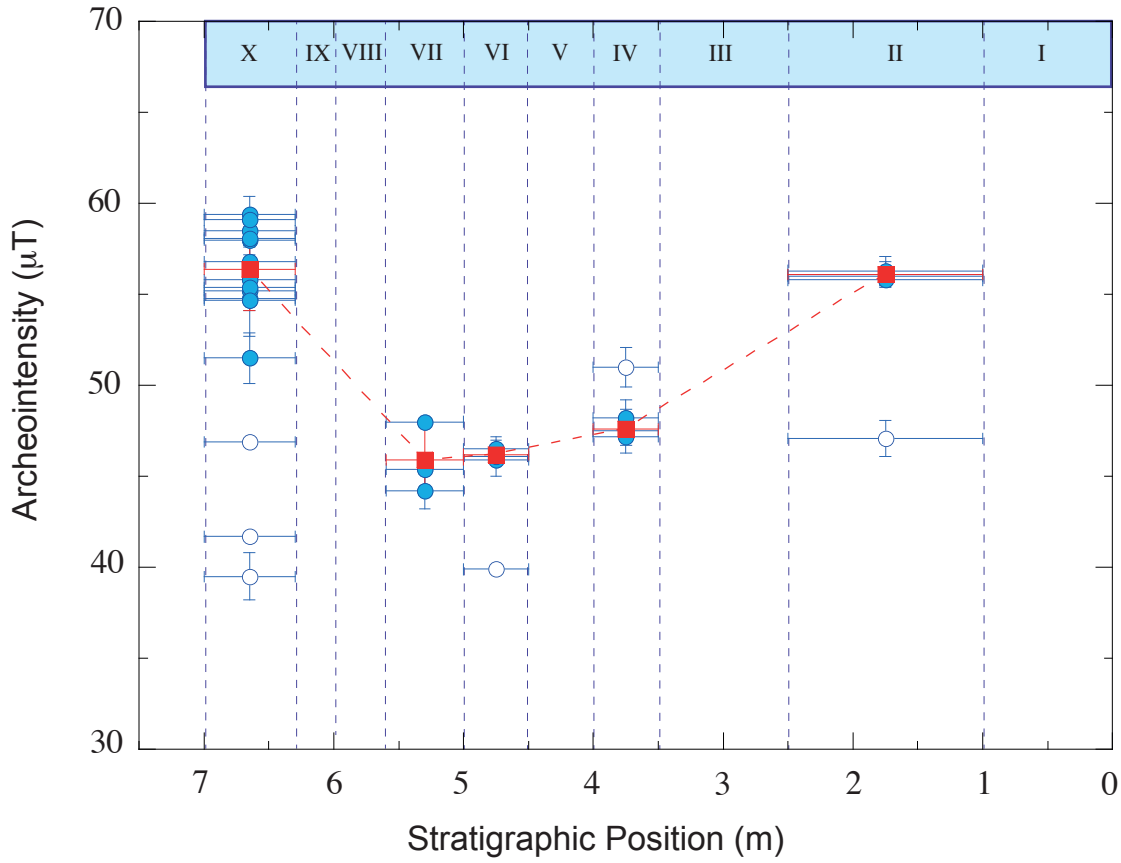

Figure 6

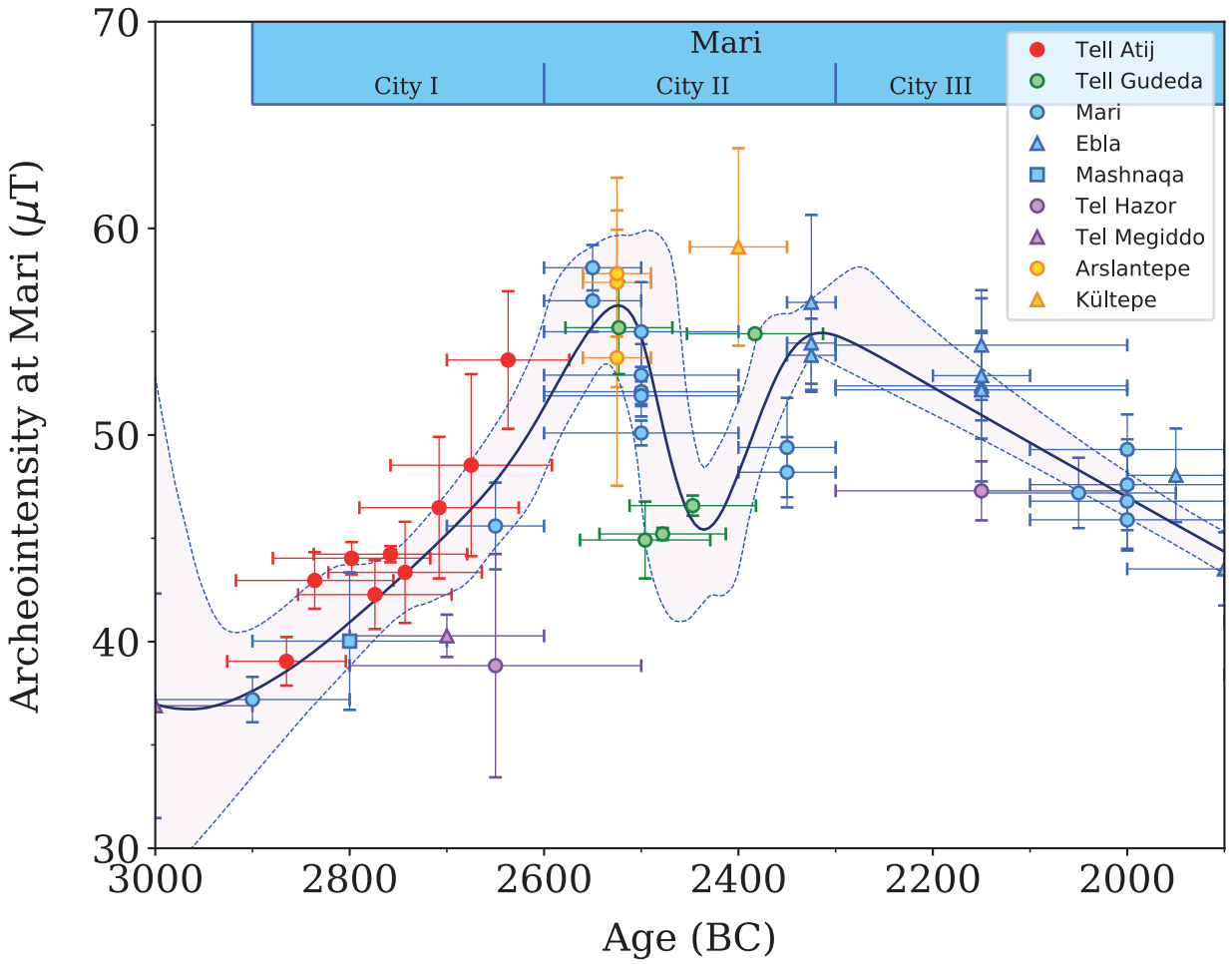
Mari
City I
City II
City III
Tell Atij
Tell Gudeda
Mari
Ebla
Mashnaqa
Tel Hazor
Tel Megiddo
Arslantepe
Kültepe
Archeointensity at Mari (μT)
70
60
50
40
30
3000
2800
2600
2400
2200
2000
Age (BC)

Figure 7

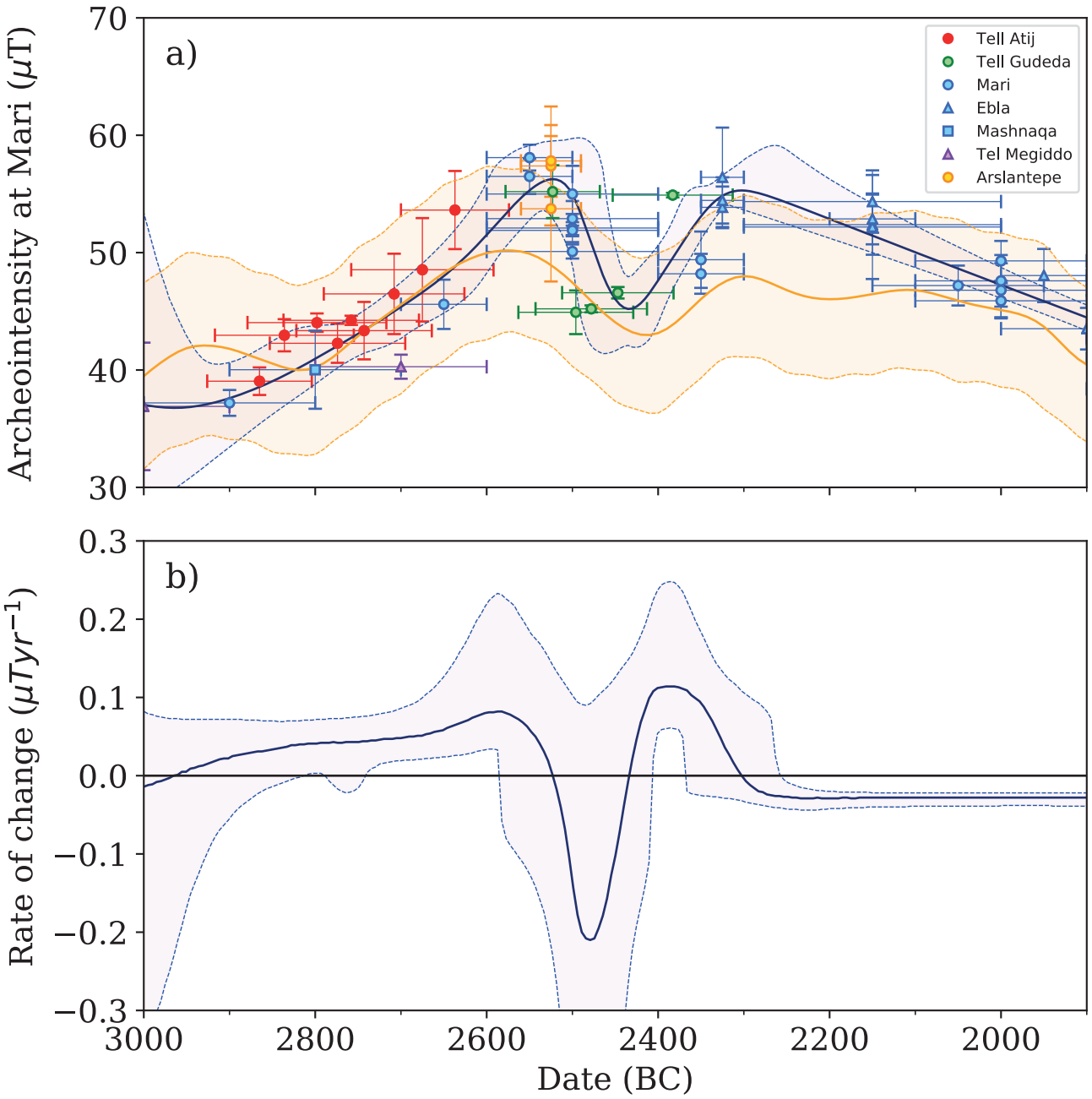
a)
b)
Tell Atij
Tell Gudeda
Mari
Ebla
Mashnaqa
Tel Megiddo
Arslantepe
Archeointensity at Mari (μT)
Rate of change (μTyr⁻¹)
Date (BC)
70
60
50
40
30
0.3
0.2
0.1
0.0
−0.1
−0.2
−0.3
3000
2800
2600
2400
2200
2000

Figure 8

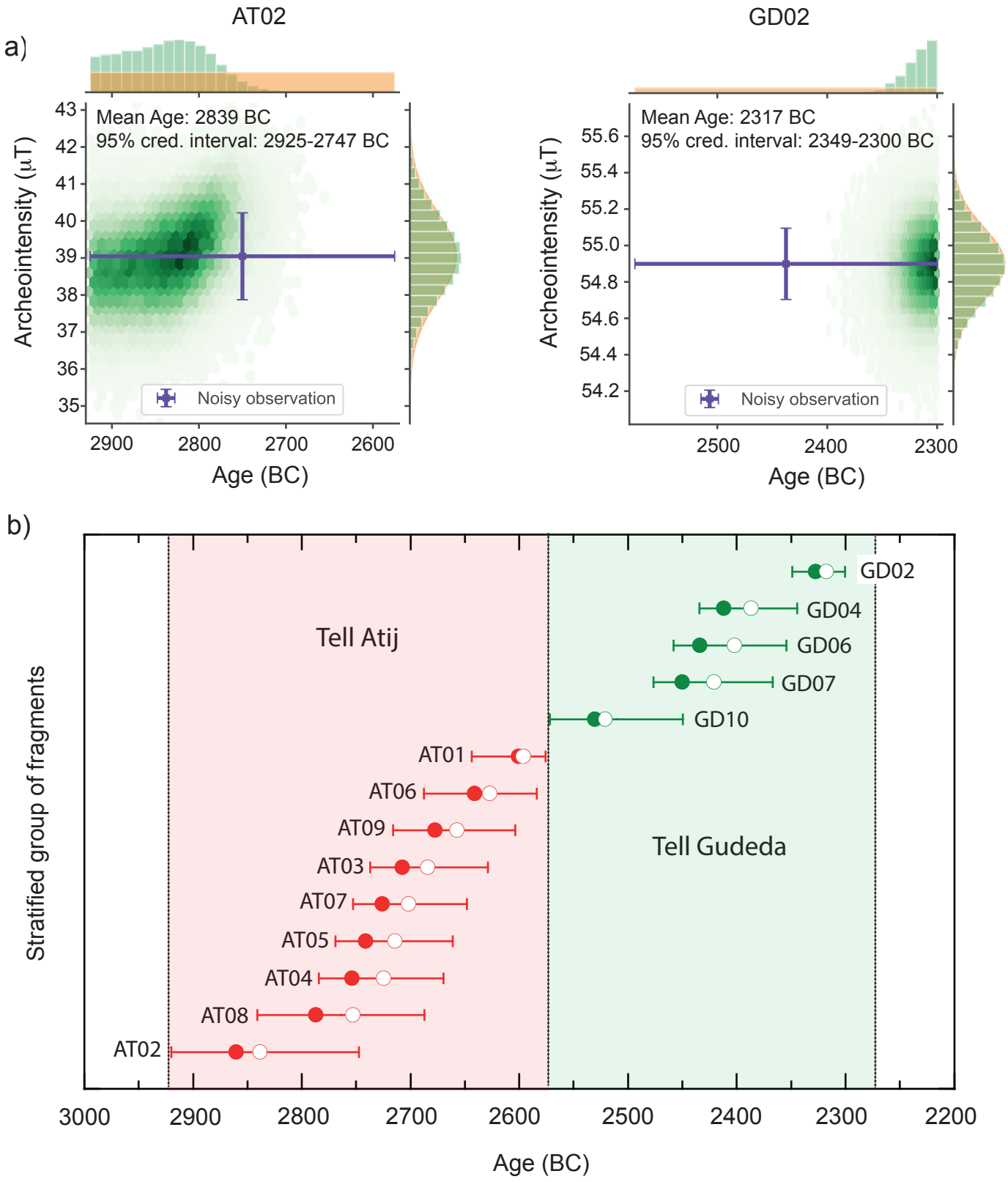
a)
AT02
GD02
Mean Age: 2839 BC
95% cred. interval: 2925-2747 BC
Mean Age: 2317 BC
95% cred. interval: 2349-2300 BC
Archeointensity (μT)
Noisy observation
Age (BC)
b)
Stratified group of fragments
Tell Atij
Tell Gudeda
GD02
GD04
GD06
GD07
GD10
AT01
AT06
AT09
AT03
AT07
AT05
AT04
AT08
AT02
Age (BC)

Figure 9

Group	Archeological level	Stratigraphic position (m)	Age (BC)	N fragment (n specimens)	Group F mean ± σ (μT)	Group F mean after 3σ test	Group F mean at Mari
Tell Atij							
AT01	I	0 - 0.85	2637 ± 63	5 (15)	50.6 ± 5.3	54.8 ± 3.4	53.5 ± 3.4
AT06	III	1.85 - 2.85	2675 ± 83	3 (9)	49.6 ± 4.5	49.6 ± 4.5	48.4 ± 4.5
AT09	IV	2.85 - 3.85	2707 ± 82	3 (9)	47.5 ± 3.5	47.5 ± 3.5	46.4 ± 3.5
AT03	VI	4.30 - 4.65	2743 ± 79	3 (9)	44.3 ± 2.5	44.3 ± 2.5	43.3 ± 2.5
AT07	VII	4.65 - 5.15	2758 ± 79	4 (12)	45.2 ± 0.4	45.2 ± 0.4	44.1 ± 0.4
AT05	VIII	5.15 - 5.65	2774 ± 79	3 (9)	43.2 ± 1.7	43.2 ± 1.7	42.2 ± 1.7
AT04	IX	5.65 - 6.65	2798 ± 81	7 (21)	44.6 ± 1.1	45.0 ± 0.8	43.9 ± 0.8
AT08	XI	6.95 - 7.70	2836 ± 81	5 (15)	42.4 ± 3.6	43.9 ± 1.4	42.9 ± 1.4
AT02	XIII	8.70 - 9.30	2865 ± 61	3 (9)	39.9 ± 1.2	39.9 ± 1.2	39.0 ± 1.2
Tell Gudeda							
GD02	II	1.00 - 2.50	2383 ± 70	5 (15)	54.3 ± 4.0	56.1 ± 0.2	54.8 ± 0.2
GD04	IV	3.50 - 4.00	2447 ± 65	4 (12)	48.5 ± 1.7	47.6 ± 0.5	46.5 ± 0.5
GD06	VI	4.50 - 5.00	2478 ± 65	4 (12)	44.6 ± 3.1	46.2 ± 0.3	45.1 ± 0.3
GD07	VII	5.00 - 5.60	2496 ± 67	3 (9)	45.9 ± 1.9	45.9 ± 1.9	44.9 ± 1.9
GD10	X	6.30 - 7.00	2523 ± 55	15 (45)	53.7 ± 6.2	56.4 ± 2.3	55.1 ± 2.3

Table 1

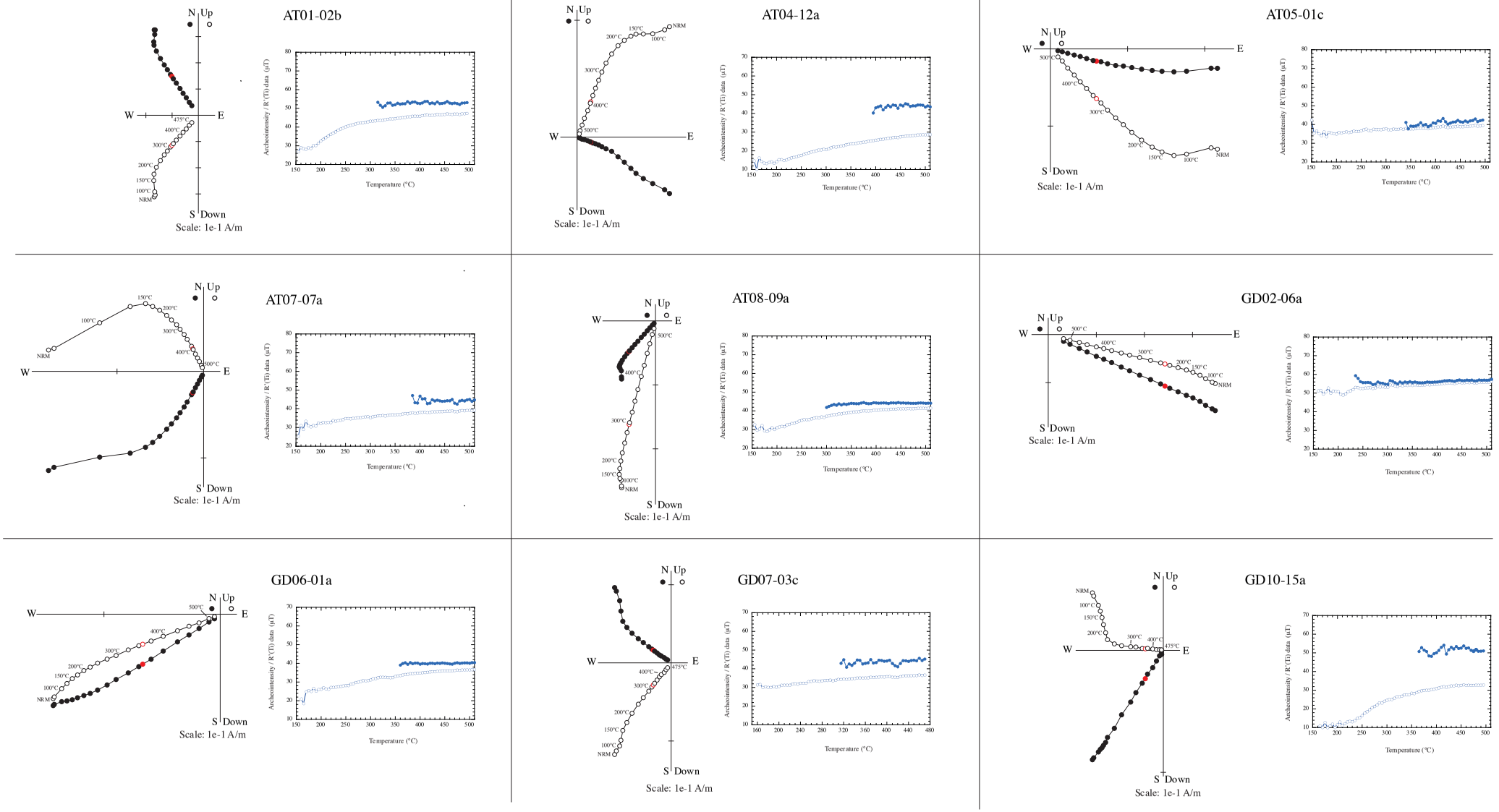
AT01-02b
N Up
W
E
S Down
Scale: 1e-1 A/m
475°C
400°C
300°C
200°C
150°C
100°C
NRM
Archeointensity / R'(Ti) data (μT)
Temperature (°C)
AT04-12a
AT05-01c
AT07-07a
AT08-09a
GD02-06a
GD06-01a
GD07-03c
GD10-15a

Figure S1

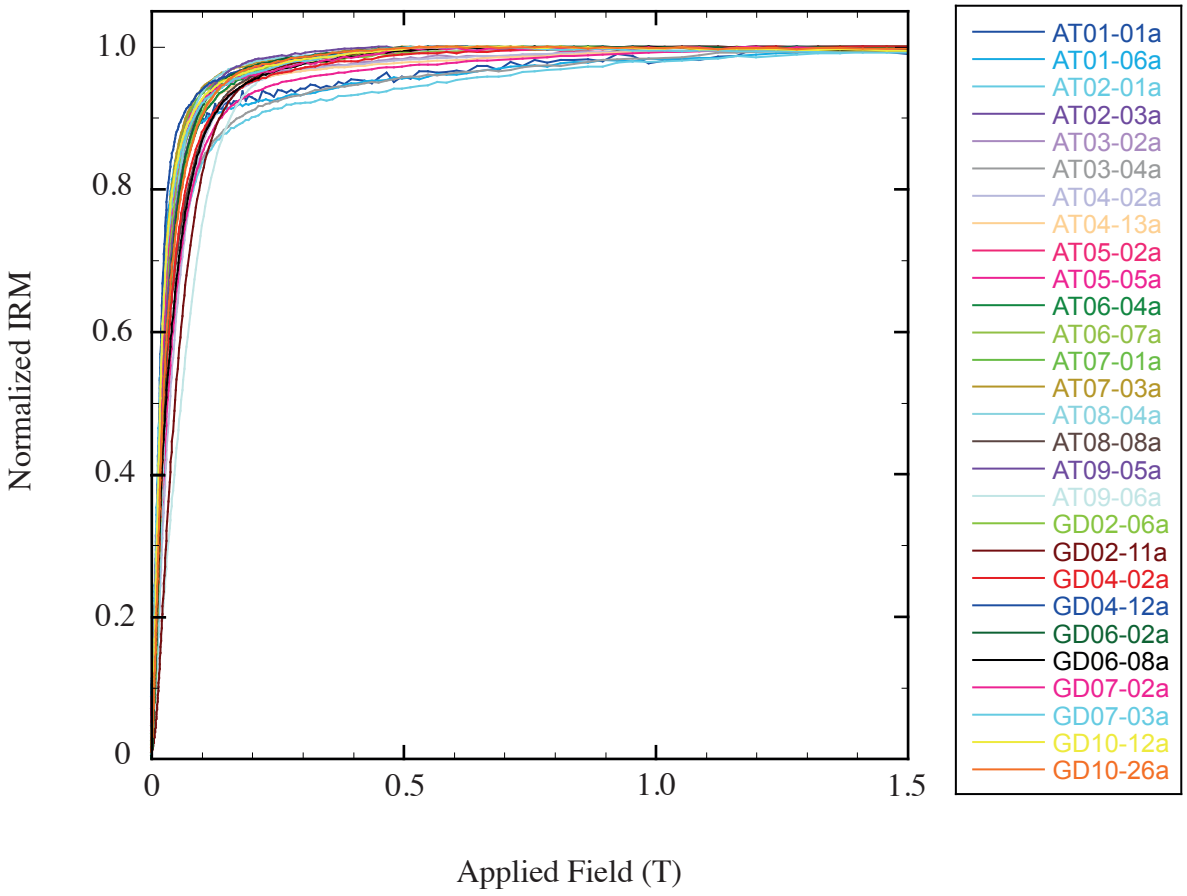
Normalized IRM
1.0
0.8
0.6
0.4
0.2
0
0
0.5
1.0
1.5
Applied Field (T)
AT01-01a
AT01-06a
AT02-01a
AT02-03a
AT03-02a
AT03-04a
AT04-02a
AT04-13a
AT05-02a
AT05-05a
AT06-04a
AT06-07a
AT07-01a
AT07-03a
AT08-04a
AT08-08a
AT09-05a
AT09-06a
GD02-06a
GD02-11a
GD04-02a
GD04-12a
GD06-02a
GD06-08a
GD07-02a
GD07-03a
GD10-12a
GD10-26a

Figure S2

a) Tell Atij

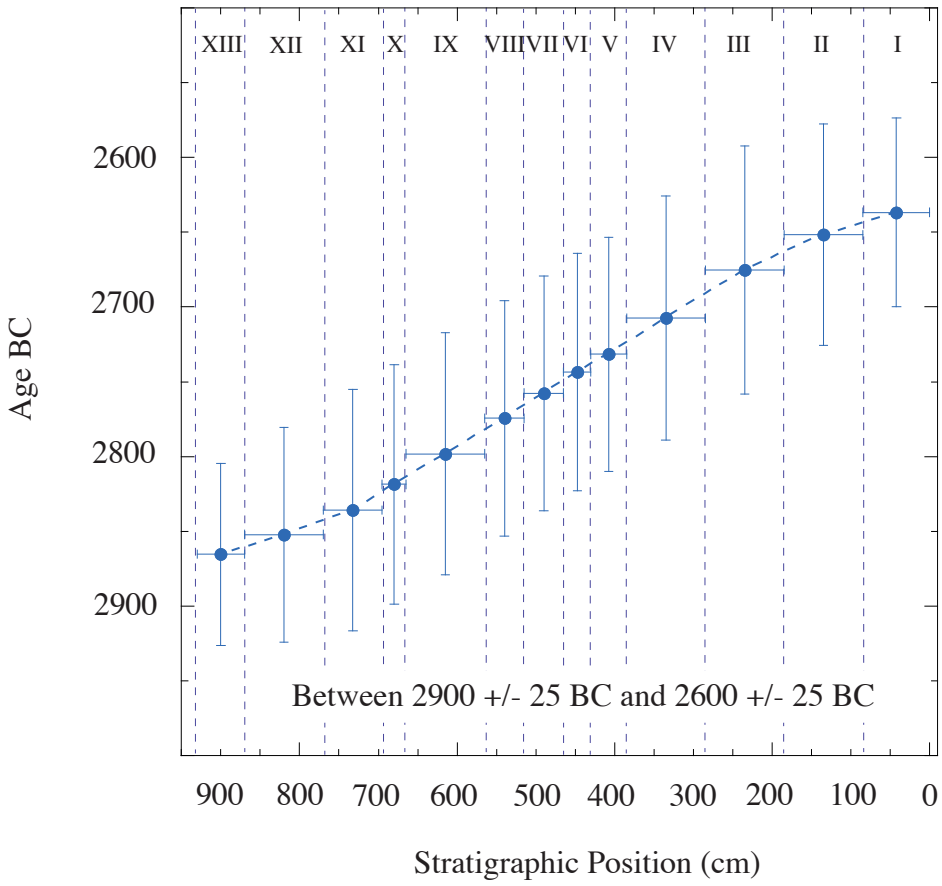

b) Tell Gudeda

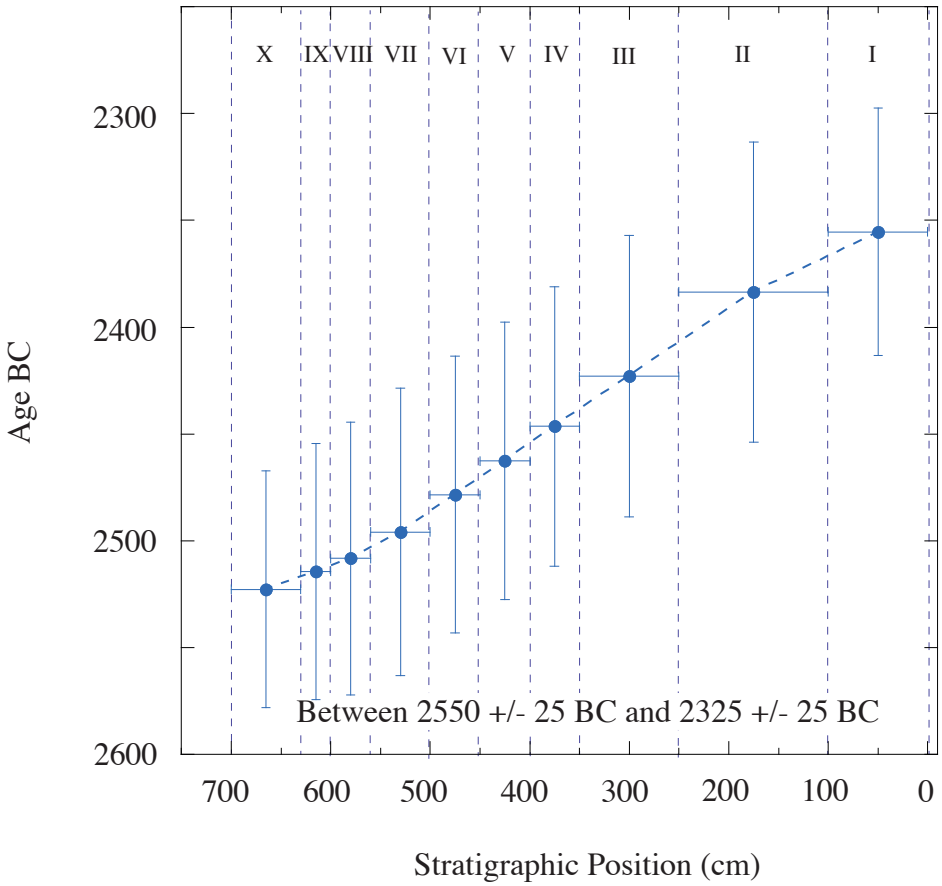

Figure S3

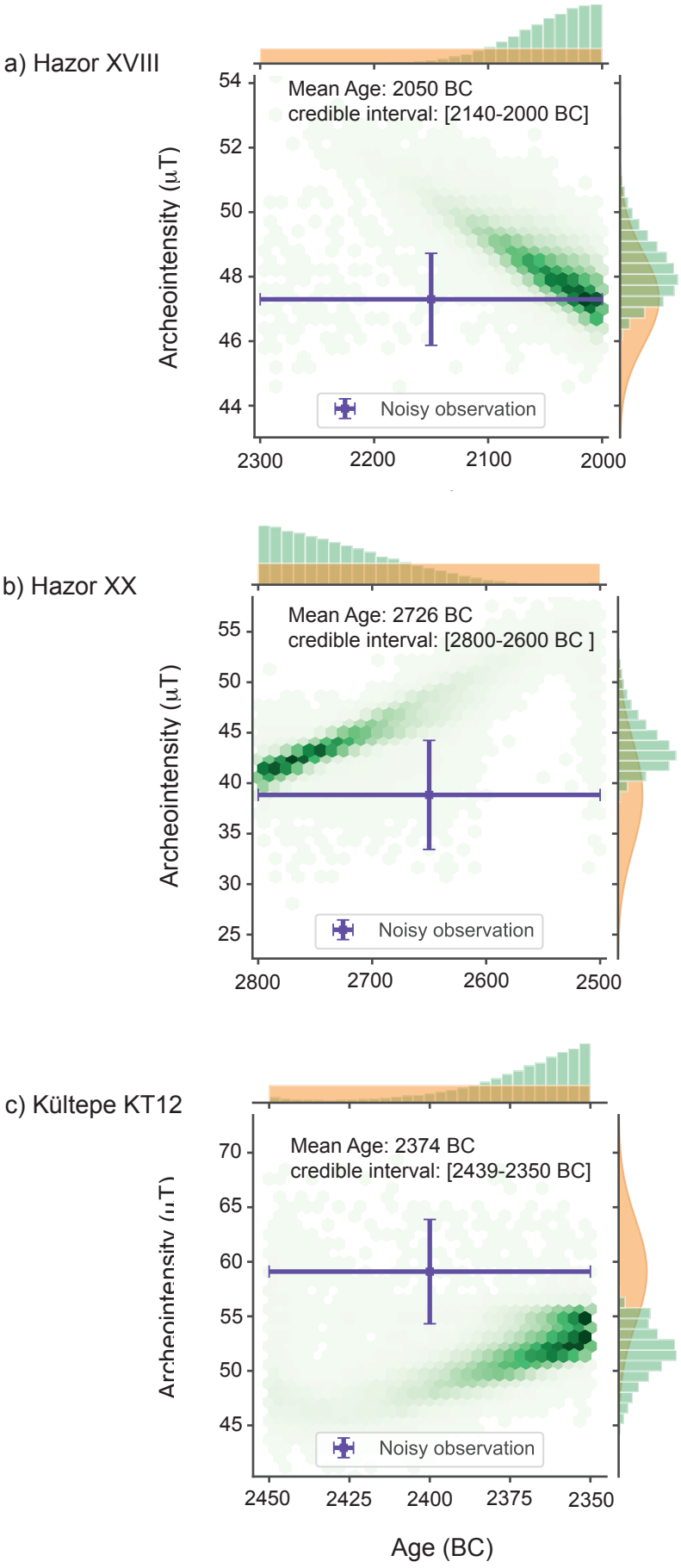
a) Hazor XVIII
Mean Age: 2050 BC
credible interval: [2140-2000 BC]
Archeointensity (μT)
54
52
50
48
46
44
Noisy observation
2300
2200
2100
2000
b) Hazor XX
Mean Age: 2726 BC
credible interval: [2800-2600 BC]
Archeointensity (μT)
55
50
45
40
35
30
25
Noisy observation
2800
2700
2600
2500
c) Kültepe KT12
Mean Age: 2374 BC
credible interval: [2439-2350 BC]
70
65
60
55
50
45
Noisy observation
2450
2425
2400
2375
2350
Age (BC)

Figure S4

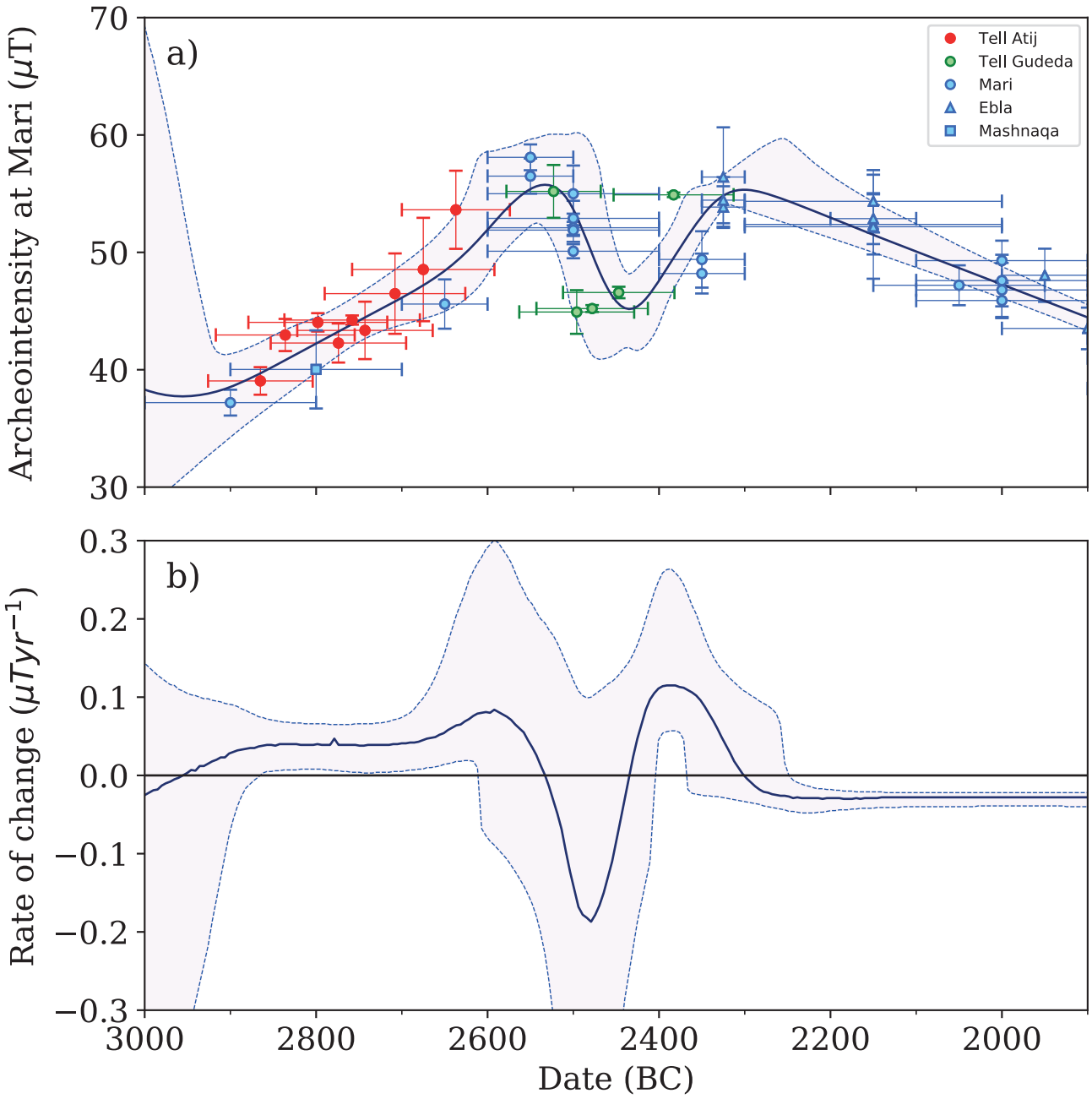
a)
b)
Tell Atij
Tell Gudeda
Mari
Ebla
Mashnaqa
Archeointensity at Mari (μT)
Rate of change ($\mu T yr^{-1}$)
Date (BC)
70
60
50
40
30
0.3
0.2
0.1
0.0
−0.1
−0.2
−0.3
3000
2800
2600
2400
2200
2000

Figure S5

Table S1. Selection criteria applied to the Triaxe archeointensity data

Selection criteria applied to the Triaxe archeointensity determinations	
At the specimen level	
• Thermal demagnetization diagram	=> Univectorial primary TRM
• "R(Ti) data" versus "Temperature" diagram	=> The R(Ti) values must be continuously increasing or ~constant from T1 (or T'1) to T2
• "R'(Ti) data" versus "Temperature" diagram	=> The R'(Ti) values must be sufficiently flat : The slope in the diagram, expressed in % through the temperature of analysis must be less than 10% (slope defined by : (R'(T2)-R'(T1 or T'1)) /(mean R'(Ti) data) => For mean computation of the R'(Ti) values : The magnetization fraction, with unblocking temperatures larger than T1(or T'1), must be at least 50%
At the fragment level	
• Coherence of the intensity values	=> Results obtained from at least 2-3 different specimens '=> Standard deviation/error ≤ 5%
At the group level	
• Number and consistency of the intensity values	=> Results obtained from at least 3 different fragments => Standard deviation around the mean ≤ 5μT